



CMS-HIN-10-004

Observation and studies of jet quenching in PbPb collisions at $\sqrt{s_{NN}} = 2.76$ TeV

The CMS Collaboration*

Abstract

Jet production in PbPb collisions at a nucleon-nucleon center-of-mass energy of 2.76 TeV was studied with the CMS detector at the LHC, using a data sample corresponding to an integrated luminosity of $6.7 \mu\text{b}^{-1}$. Jets are reconstructed using the energy deposited in the CMS calorimeters and studied as a function of collision centrality. With increasing collision centrality, a striking imbalance in dijet transverse momentum is observed, consistent with jet quenching. The observed effect extends from the lower cut-off used in this study (jet $p_T = 120$ GeV/ c) up to the statistical limit of the available data sample (jet $p_T \approx 210$ GeV/ c). Correlations of charged particle tracks with jets indicate that the momentum imbalance is accompanied by a softening of the fragmentation pattern of the second most energetic, away-side jet. The dijet momentum balance is recovered when integrating low transverse momentum particles distributed over a wide angular range relative to the direction of the away-side jet.

Submitted to Physical Review C

*See Appendix A for the list of collaboration members

1 Introduction

High-energy collisions of heavy ions allow the fundamental theory of the strong interaction — Quantum Chromodynamics (QCD) — to be studied under extreme temperature and density conditions. A new form of matter [1–4] formed at energy densities above $\sim 1 \text{ GeV}/\text{fm}^3$ is predicted in Lattice QCD calculations [5]. This quark-gluon plasma (QGP) consists of an extended volume of deconfined and chirally-symmetric quarks and gluons.

Heavy ion collisions at the Large Hadron Collider (LHC) are expected to produce matter at energy densities exceeding any previously explored in experiments conducted at particle accelerators. One of the first experimental signatures suggested for QGP studies was the suppression of high-transverse-momentum (p_T) hadron yields resulting from energy loss suffered by hard-scattered partons passing through the medium [6]. This parton energy loss is often referred to as “jet quenching”. The energy lost by a parton provides fundamental information on the thermodynamical and transport properties of the traversed medium, which is now believed to be strongly coupled as opposed to an ideal gas of quarks and gluons (recent reviews: [7, 8]). Results from nucleus-nucleus collisions at the Relativistic Heavy Ion Collider (RHIC) [9–12] have shown evidence for the quenching effect through the suppression of inclusive high- p_T hadron production and the modification of high- p_T dihadron angular correlations when compared to the corresponding results in much smaller systems, especially proton-proton collisions. Preliminary results for fully reconstructed jets at RHIC, measured in AuAu collisions at $\sqrt{s_{NN}} = 200 \text{ GeV}$ [13–16], also hint at broadened jet shapes due to medium-induced gluon radiation.

Studying the modification of jets has long been proposed as a particularly useful tool for probing the QGP properties [17, 18]. Of particular interest are the dominant “dijets”, consisting of the most energetic (“leading”) and second most energetic (“subleading”) jets. At leading order (LO) and in the absence of parton energy loss, the two jets have equal p_T with respect to the beam axis and are emitted very close to back-to-back in azimuth ($\Delta\phi_{\text{dijet}} = |\phi_{\text{jet1}} - \phi_{\text{jet2}}| \approx \pi$). However, medium-induced gluon emission in the final state can significantly alter the energy balance between the two highest- p_T jets and may give rise to large deviations from $\Delta\phi_{\text{dijet}} \approx \pi$. Such medium effects in nuclear interactions are expected to be much larger than those due to higher-order gluon radiation, which is also present for jet events in pp collisions. The study of medium-induced modifications of dijet properties can therefore shed light on the transport properties of the QCD medium formed in heavy ion collisions.

The dijet analysis presented in this paper was performed using the data collected in 2010 from PbPb collisions at a nucleon-nucleon center-of-mass energy of $\sqrt{s_{NN}} = 2.76 \text{ TeV}$ at the Compact Muon Solenoid (CMS) detector. The CMS detector has a solid angle acceptance of nearly 4π and is designed to measure jets and energy flow, an ideal feature for studying heavy ion collisions. A total integrated (PbPb) luminosity of $8.7 \mu\text{b}^{-1}$ was collected, of which $6.7 \mu\text{b}^{-1}$ has been included in this analysis. Recently, related results on a smaller data sample ($1.7 \mu\text{b}^{-1}$) have been reported by ATLAS [19].

Jets were reconstructed based on their energy deposits in the CMS calorimeters. In general, the jet quenching effect on partons traversing the medium with different path lengths will lead to modifications in the observed dijet energy balance due to a combination of two effects: the radiated energy can fall outside the area used for the determination of the jet energy, and the energy can be shifted towards low momentum particles, which will not be detected in the calorimetric energy measurement. Such unbalanced events are easy to detect visually even at the level of event displays, and numerous examples were in fact seen during the first days of data taking (e.g. Fig. 1).

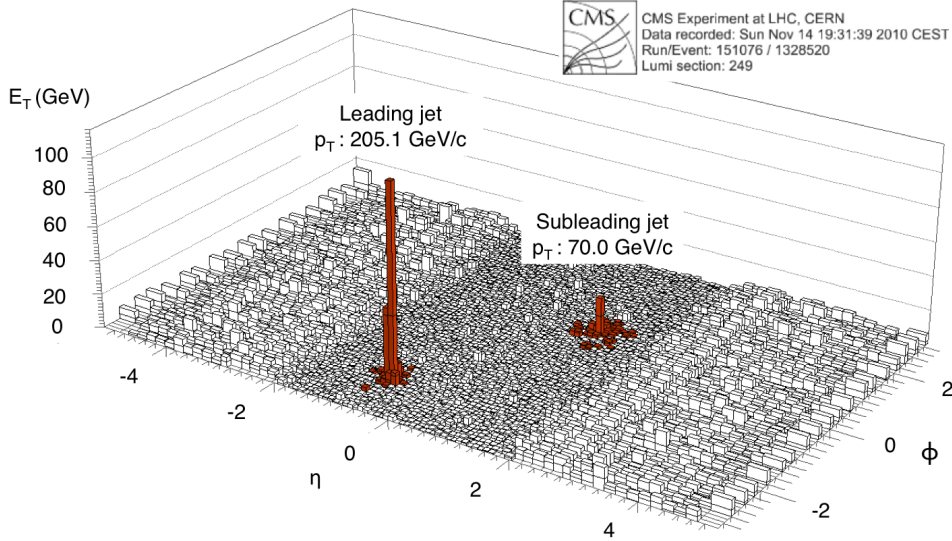


Figure 1: Example of an unbalanced dijet in a PbPb collision event at $\sqrt{s_{NN}} = 2.76$ TeV. Plotted is the summed transverse energy in the electromagnetic and hadron calorimeters vs. η and ϕ , with the identified jets highlighted in red, and labeled with the corrected jet transverse momentum.

The data provide information on the evolution of the dijet imbalance as a function of both collision centrality (i.e., the degree of overlap of the two colliding nuclei) and the energy of the leading jet. By correlating the dijets detected in the calorimeters with charged hadrons reconstructed in the high-resolution tracker system, the modification of the jet fragmentation pattern can be studied in detail, thus providing a deeper insight into the dynamics of the jet quenching phenomenon.

The paper is organized as follows: the experimental setup, event triggering, selection and characterization, and jet reconstruction are described in Section 2. Section 3 presents the results and a discussion of systematic uncertainties, followed by a summary in Section 4.

2 Experimental method

The CMS detector is described in detail elsewhere [20]. The calorimeters provide hermetic coverage over a large range of pseudorapidity, $|\eta| < 5.2$, where $\eta = -\ln[\tan(\theta/2)]$ and θ is the polar angle relative to the particle beam. In this study, jets are identified primarily using the energy deposited in the lead-tungstate crystal electromagnetic calorimeter (ECAL) and the brass/scintillator hadron calorimeter (HCAL) covering $|\eta| < 3$. In addition, a steel/quartz-fiber Cherenkov calorimeter, called Hadron Forward (HF), covers the forward rapidities $3 < |\eta| < 5.2$ and is used to determine the centrality of the PbPb collision. Calorimeter cells are grouped in projective towers of granularity in pseudorapidity and azimuthal angle given by $\Delta\eta \times \Delta\phi = 0.087 \times 0.087$ at central rapidities, having a coarser segmentation at forward rapidities. The central calorimeters are embedded in a solenoid with 3.8 T central magnetic field. The event display shown in Fig. 1 illustrates the projective calorimeter tower granularity over the full pseudorapidity range. The CMS tracking system, located inside the calorimeter, consists of pixel and silicon-strip layers covering $|\eta| < 2.5$, and provides track reconstruction down to $p_T \approx 100$ MeV/c, with a track momentum resolution of about 1% at $p_T = 100$ GeV/c. A set of scintillator tiles, the Beam Scintillator Counters (BSC), are mounted on the inner side of the

HF calorimeters for triggering and beam-halo rejection. CMS uses a right-handed coordinate system, with the origin located at the nominal collision point at the center of the detector, the x -axis pointing towards the center of the LHC ring, the y -axis pointing up (perpendicular to the LHC plane), and the z -axis along the counterclockwise beam direction. The detailed Monte Carlo (MC) simulation of the CMS detector response is based on GEANT4 [21].

2.1 Data samples and triggers

The expected cross section for hadronic inelastic PbPb collisions at $\sqrt{s_{NN}} = 2.76$ TeV is 7.65 b, corresponding to the chosen Glauber MC parameters described in Section 2.3. In addition, there is a sizable contribution from large impact parameter ultra-peripheral collisions (UPC) that lead to the electromagnetic breakup of one, or both, of the Pb nuclei [22]. particles per unit of pseudorapidity, depending on the impact parameter.

For online event selection, CMS uses a two-level trigger system: Level-1 (L1) and High Level Trigger (HLT). The events for this analysis were selected using an inclusive single-jet trigger that required an L1 jet with $p_T > 30$ GeV/ c and an HLT jet with $p_T > 50$ GeV/ c , where neither p_T value was corrected for the p_T -dependent calorimeter energy response discussed in Section 2.4.3. The efficiency of the jet trigger is shown in Fig. 2 (a) for leading jets with $|\eta| < 2$ as a function of their corrected p_T . The efficiency is defined as the ratio of the number of triggered events over the number of minimum bias events (described below). The trigger becomes fully efficient for collisions with a leading jet with corrected p_T greater than 100 GeV/ c .

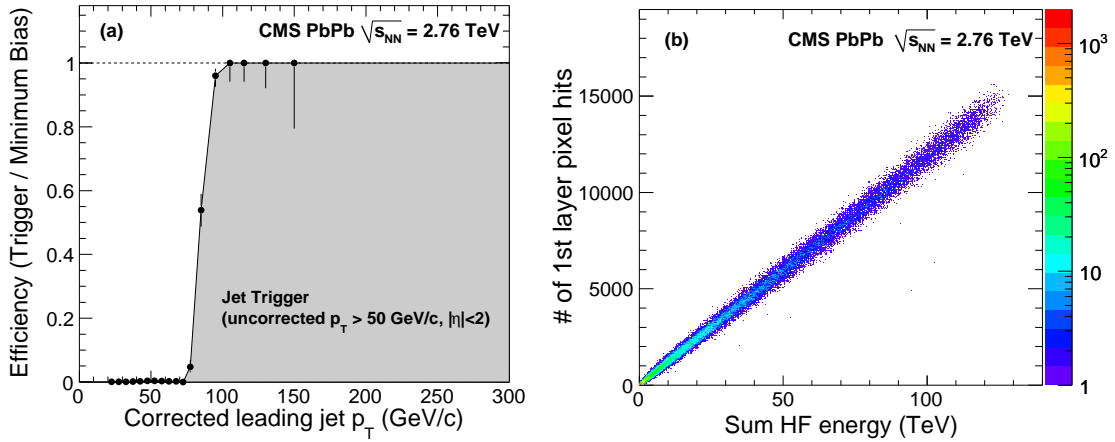


Figure 2: (a) Efficiency curve for the HLT 50 GeV/ c single-jet trigger, as a function of the corrected leading jet transverse momentum. Error bars shown are statistical. (b) Correlation between the number of pixel hits and HF total energy for a single run containing 60 k minimum bias events, after selections as described in the text.

In addition to the jet data sample, a minimum bias event sample was collected using coincidences between the trigger signals from the $+z$ and $-z$ sides of either the BSC or the HF. This trigger has an efficiency of more than 97% for hadronic inelastic collisions. In order to suppress non-collision related noise, cosmic rays, double-firing triggers, and beam backgrounds, the minimum bias and jet triggers used in this analysis were required to fire in time with the presence of both colliding ion bunches in the interaction region. It was checked that the events selected by the jet trigger described above also satisfy all triggers and selections imposed for minimum bias events. The total hadronic collision rate varied between 1 and 210 Hz, depending on the number of colliding bunches (between 1×1 and 129×129) and on the bunch intensity.

2.2 Event selection

In order to select a pure sample of inelastic hadronic collisions for analysis, a number of offline selections were applied to the triggered event sample, removing contaminations from UPC events and non-collision beam backgrounds (e.g. beam-gas). Table 1 shows the number of events remaining after the various selection criteria are applied. First, beam halo events were vetoed based on the timing of the $+z$ and $-z$ BSC signals. Then, to veto UPC and beam-gas events, an offline HF coincidence of at least three towers on each side of the interaction point was required, with a total deposited energy of at least 3 GeV. Next, a reconstructed vertex was required with at least two tracks of $p_T > 75$ MeV/ c , consistent with the transverse beam spot position and the expected collision region along the z -axis. Finally, to further reject beam-gas and beam-scraping events, the length of pixel clusters along the beam direction were required to be compatible with particles originating from the primary vertex. This last selection is identical to the one used for the study of charged hadron pseudorapidity density and p_T spectrum in 7 TeV pp collisions [23]. Figure 2 (b) shows the correlation between the total energy deposited in the HF calorimeters and the number of hits in the first layer of the silicon pixel barrel detector after these event selections. A tight correlation between the two detectors is observed, with very few of the events showing HF energy deposits that deviate significantly (at any given number of pixel hits) from the expectations for hadronic PbPb collisions. This correlation is important to verify the selection of a pure collision event sample, and also to validate the HF energy sum as a measure of event centrality (Section 2.3).

Starting from inelastic hadron collisions based on the selections described above, the basic offline selection of events for the analysis is the presence of a leading calorimeter jet in the pseudorapidity range of $|\eta| < 2$ with a corrected jet $p_T > 120$ GeV/ c . By selecting these leading jets we avoid possible biases due to inefficiencies close to the trigger threshold. Furthermore, the selection of a rather large leading jet momentum expands the range of jet momentum imbalances that can be observed between the leading and subleading jets, as the subleading jets need a minimum momentum of $p_T > 35$ – 50 GeV/ c to be reliably detected above the high-multiplicity underlying event in PbPb collisions (Section 2.4). In order to ensure high quality dijet selection, kinematic selection cuts were applied. The azimuthal angle between the leading and subleading jet was required to be at least $2\pi/3$. Also, we require a minimum p_T of $p_{T,1} > 120$ GeV/ c for leading jets and of $p_{T,2} > 50$ GeV/ c for subleading jets. No explicit requirement is made either on the presence or absence of a third jet in the event. Prior to jet finding on the selected events, a small contamination of noise events from uncharacteristic ECAL and HCAL detector responses was removed using signal timing, energy distribution, and pulse-shape information [24, 25]. As a result, about 2.4% of the events were removed from the sample.

2.3 Centrality determination

For the analysis of PbPb events, it is important to know the “centrality” of the collision, i.e., whether the overlap of the two colliding nuclei is large or small. In this analysis, the observable used to determine centrality is the total energy from both HF calorimeters. The distribution of the HF signal used in this analysis is shown in Fig. 3 (a). The shape of the energy distribution is characteristic of all observables related to (soft) particle production in heavy ion collisions. The more frequent peripheral events with large impact parameter produce very few particles, while the central ones with small impact parameter produce many more particles because of the increased number of nucleon-nucleon interactions.

The distribution of this total energy was used to divide the event sample into 40 centrality bins, each representing 2.5% of the total nucleus-nucleus interaction cross section. Because

Table 1: Event selection criteria used for this analysis. The percentage of events remaining after each criterion, listed in the last column, are with respect to the previous criterion (the event selection criteria are applied in the indicated sequence).

Criterion	Events remaining	% of events remaining
Jet triggered events ($p_T^{\text{uncorr}} > 50 \text{ GeV}/c$)	149 k	100.00
No beam halo, based on the BSC	148 k	99.61
HF offline coincidence	111 k	74.98
Reconstructed vertex	110 k	98.97
Beam-gas removal	110 k	99.78
ECAL cleaning	107 k	97.66
HCAL cleaning	107 k	99.97
≥ 2 jets with $p_T > 35 \text{ GeV}/c$ and $ \eta < 2$	71.9k	67.07
Leading jet $p_{T,1} > 120 \text{ GeV}/c$	4 216	5.86
Subleading jet $p_{T,2} > 50 \text{ GeV}/c$	3 684	87.38
$\Delta\phi_{12}$ of 2 jets $> 2\pi/3$	3 514	95.39

of inefficiencies in the minimum bias trigger and event selection, the measured multiplicity distribution does not represent the full interaction cross section. MC simulations were used to estimate the distribution in the regions where events are lost. Comparing the simulated distribution to the measured distribution, it is estimated that the minimum bias trigger and event selection efficiency is $97 \pm 3\%$.

For the jet analysis, these fine-grained bins were combined into five larger bins corresponding to the most central 10% of the events (i.e., smallest impact parameter), the next most central 10% of the events (denoted 10–20%), and further bins corresponding to the 20–30%, 30–50%, and 50–100% selections of the total hadronic cross section.

Simulations can be used to correlate centrality, as quantified using the fraction of the total interaction cross section, with more detailed properties of the collision. The two most commonly used physical quantities are the total number of nucleons in the two lead (^{208}Pb) nuclei which experienced at least one inelastic collision, denoted N_{part} , and the total number of binary nucleon-nucleon collisions, N_{coll} .

The centrality bins can be correlated to the impact parameter, b , and to average values and variances of N_{part} and N_{coll} using a calculation based on a Glauber model in which the nucleons are assumed to follow straight-line trajectories as the nuclei collide (for a review, see [26]). The bin-to-bin smearing of the results of these calculations due to the finite resolution and fluctuations in the HF energy measurement was obtained from fully simulated and reconstructed MC events generated with the AMPT event generator [27]. Standard parameters of the Woods-Saxon function used to model the distribution of nucleons in the Pb nuclei were used [28]. The nucleon-nucleon inelastic cross section, which is used to determine how close the nucleon trajectories need to be in order for an interaction to occur, was taken to be $64 \pm 5 \text{ mb}$, based on a fit of the existing data for total and elastic cross-sections in proton-proton and proton-antiproton collisions [29]. The uncertainties in the parameters involved in these calculations contribute to the systematic uncertainty in N_{part} and N_{coll} for a given bin. The other source of uncertainty in the centrality parameters comes from the determination of the event selection efficiency.

Using the procedure outlined above, the mean and spread (RMS) values of the impact parameter, N_{part} , and N_{coll} for the five bins used in this analysis, and their systematic uncertainties,

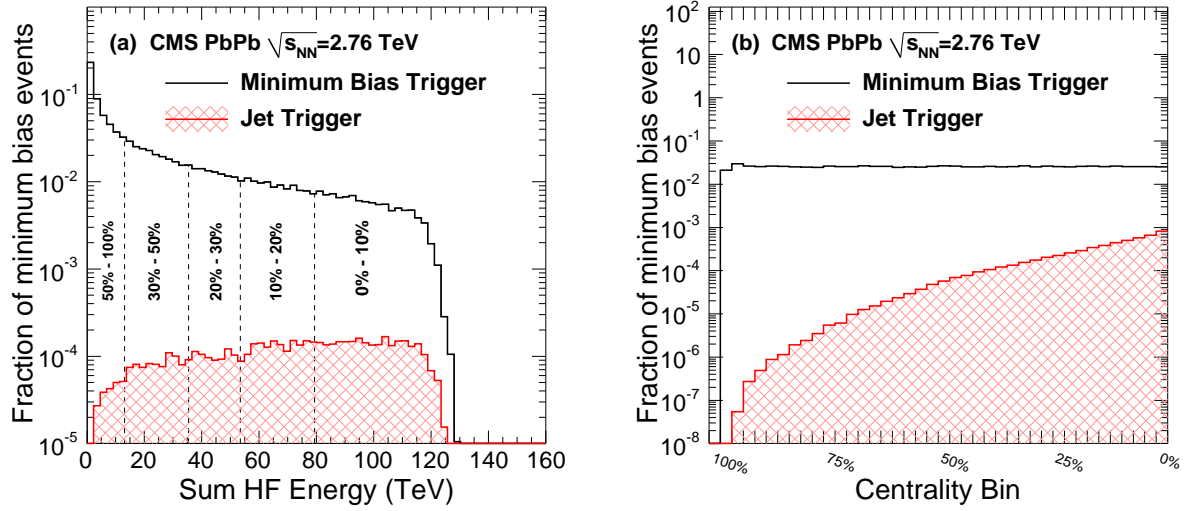


Figure 3: (a) Probability distribution of the total HF energy for minimum bias collisions (black open histogram). The five regions correspond to the centrality ranges used in this analysis. Also shown is the HF energy distribution for the subset of events passing the HLT jet trigger (red hatched histogram). (b) Distribution of the fraction of events in the 40 centrality bins for minimum bias (black open histogram) and HLT jet triggered (red hatched histogram) events. The centrality-bin labels run from 100% for the most peripheral to 0% for the most central events.

were extracted and are listed in Table 2. The RMS values for the centrality parameters are due to their correlation with the percentage cross section and the width of the chosen centrality bins.

It is important to note that the selection of rare processes, such as the production of high- p_T jets, leads to a strong bias in the centrality distribution of the underlying events towards more central collisions, for which N_{coll} is very large. This can be seen in Fig. 3 (a), where the HF energy distribution for events selected by the jet trigger is shown in comparison to that for minimum bias events. The bias can be seen more clearly in Fig. 3 (b), where the distribution of minimum bias and jet-triggered events in the 40 centrality bins is shown.

Table 2: Mean and RMS values for the distributions of impact parameter, b , number of participating nucleons, N_{part} , and number of nucleon-nucleon collisions, N_{coll} , for the centrality bins used in this analysis. The RMS values represent the spread of each quantity within the given bins due to the range of percentage cross section included.

Centrality	b mean (fm)	b RMS (fm)	N_{part} mean	N_{part} RMS	N_{coll} mean	N_{coll} RMS
0–10%	3.4 ± 0.1	1.2	355 ± 3	33	1484 ± 120	241
10–20%	6.0 ± 0.2	0.8	261 ± 4	30	927 ± 82	183
20–30%	7.8 ± 0.2	0.6	187 ± 5	23	562 ± 53	124
30–50%	9.9 ± 0.3	0.8	108 ± 5	27	251 ± 28	101
50–100%	13.6 ± 0.4	1.6	22 ± 2	19	30 ± 5	35

2.4 Jet reconstruction in PbPb collisions

2.4.1 Jet algorithm

The baseline jet reconstruction for heavy ion collisions in CMS is performed with an iterative cone algorithm modified to subtract the soft underlying event on an event-by-event basis [30]. Each cone is selected with a radius $\Delta R = \sqrt{\Delta\phi^2 + \Delta\eta^2} = 0.5$ around a seed of minimum transverse energy of 1 GeV. The underlying event subtraction algorithm is a variant of an iterative “noise/pedestal subtraction” technique [31]. Initially, the mean value, $\langle E_{\text{cell}} \rangle$, and dispersion, $\sigma(E_{\text{cell}})$, of the energies recorded in the calorimeter cells are calculated for all rings of cells that have at least 0.3 GeV transverse energy deposit at constant pseudorapidity. The algorithm subtracts $\langle E_{\text{cell}} \rangle + \sigma(E_{\text{cell}})$ from each cell. If a cell energy is negative after subtraction, the value is set to zero. Subtracting the mean plus the dispersion, as opposed to simply the mean, compensates for the bias caused by the “zeroing” of negative-energy cells. Jets are then reconstructed, using a standard iterative cone algorithm [32, 33], from the remaining cells with non-zero energy. In a second iteration, the pedestal function is recalculated using only calorimeter cells outside the area covered by reconstructed high- p_T jets ($p_T > 10$ GeV/c). The threshold of 10 GeV/c was chosen in studies optimizing the final extracted jet p_T resolution. The cell energies are updated with the new pedestal function (again subtracting mean plus dispersion) and the jets are reconstructed again, using the updated calorimeter cells. The performance of this algorithm is documented in Ref. [30]. Jet corrections for the calorimeter response have been applied, as determined in studies for pp collisions [34]. When applying the algorithm to PbPb data, the subtracted background energy for $R = 0.5$ jet cones ranges from 6–13 GeV for peripheral events (centrality bins 50–100%) to 90–130 GeV for central collisions (0–10%), before applying jet energy scale corrections.

To perform a cross-check of the main results, the anti- k_T algorithm [35] with a resolution parameter of 0.5 was used to reconstruct jets, as was done for the pp reference measurements presented here. The energy attributed to the underlying event was estimated and subtracted using the “average energy per jet area” procedure provided by the FASTJET package [36, 37]. In order to eliminate biases in the underlying event estimation, an η -strip of total width $\Delta\eta = 1.6$ centered on the jet position was used, with the two highest energy jets in each event excluded [38]. In addition, the anti- k_T jets were reconstructed based on particle flow objects [39, 40] instead of calorimeter-only information. A good agreement was found with the calorimeter-based, iterative cone algorithm results.

2.4.2 Simulated data samples

For the analysis of dijet properties in PbPb events, it is crucial to understand how the jet reconstruction is modified in the presence of the high multiplicity of particles produced in the PbPb underlying event. The jet-finding performance was studied using dijets in pp collisions simulated with the PYTHIA event generator (version 6.423, tune D6T) [41], modified for the isospin content of the colliding nuclei [42]. In order to enhance the number of Pythia dijets in the momentum range studied, a minimum \hat{p}_T selection of 80 GeV/c was used. Lower \hat{p}_T selections, as discussed in [43], were also investigated and found to agree with the $\hat{p}_T = 80$ GeV/c results within uncertainties. The PYTHIA dijet events were processed with the full detector simulation and analysis chain. Additional samples were produced in which the PYTHIA dijet events were embedded into a minimum bias selection of PbPb events at the raw data level. For this embedding procedure, both real PbPb data events (PYTHIA+DATA), and PbPb events simulated with the HYDJET event generator [42] (PYTHIA+HYDJET) were used. The HYDJET parameters were tuned to reproduce the total particle multiplicities at all centralities and to approximate

the underlying event fluctuations seen in data. The HYDJET events included the simulation of hard-scattering processes for which radiative parton energy loss was simulated, but collisional energy loss was turned off [42]. Both embedded samples were propagated through the standard reconstruction and analysis chain.

The PYTHIA+DATA sample was used in several ways for studies of calorimeter jets. First, by matching the same PYTHIA dijet event reconstructed with and without the PbPb underlying event, the degradation of the jet p_T and position resolution, the jet p_T scale, and the jet-finding efficiency were determined as a function of collision centrality and jet p_T (Section 2.4.3). In addition, PYTHIA+DATA events were compared to non-embedded PYTHIA for dijet observables such as azimuthal correlations and momentum balance distributions. Finally, to separate effects due to the medium itself from effects simply due to reconstructing jets in the complicated environment of the underlying PbPb event, a direct comparison of results for PYTHIA+DATA and actual data events was made (Section 3.1).

The PYTHIA+HYDJET sample was used for studies of track momentum balance and track-jet correlations (Sections 3.2 and 3.3), where access to the full MC particle level (truth) information for charged tracks is important for systematic studies.

2.4.3 Jet-finding performance

A detailed characterization of the CMS calorimeter jet-finding performance in pp collisions can be found in [44]. The dependence of the jet energy scale and of the jet energy resolution on centrality was determined using the PYTHIA+DATA sample (Fig. 4, standard pp jet energy corrections are applied). In this study, reconstructed jets were matched to the closest generator-level jet in η - ϕ within a cone of $\Delta R = 0.3$. The residual jet energy scale dependence and the relative jet energy resolution are derived from the mean and standard deviation of the approximately Gaussian distributions of the ratio of the reconstructed calorimeter jet transverse momentum p_T^{CaloJet} and the transverse momentum of jets reconstructed based on event generator level final state particles p_T^{GenJet} . For peripheral events in the 50–100% centrality selection, the jet energies are under-corrected by 5% after applying the standard pp jet energy corrections, and the jet energy resolution is found to be about 15% worse than in pp collisions. For the most central events, the large transverse energy per unit area of the underlying event leads to an over-correction of low- p_T jet energies by up to 10% and a degradation of the relative resolution by about 30% to $\sigma(p_T^{\text{CaloJet}}/p_T^{\text{GenJet}}) = 0.16$ at $p_T = 100$ GeV/c. The effect of the underlying event on the jet angular resolution was also studied. Integrated over jet $p_T > 50$ GeV/c, the angular resolution in ϕ worsens from 0.03 for peripheral events (50–100%) to 0.04 for central events (0–10%), while the resolution in η changes from 0.02 to 0.03 over the same centrality range.

The jet reconstruction efficiency as a function of jet p_T and centrality was extracted from the PYTHIA+DATA sample as well, with the results shown in Fig. 5. For peripheral events, a jet-finding efficiency of 95% was found for a jet $p_T = 50$ GeV/c, while for central collisions the efficiency drops to 88% at the same p_T . Jets with $p_T > 70$ GeV/c are found with an efficiency greater than 97% for all collision centralities. No correction for the inefficiency near the threshold was applied in the subsequent analysis, as the effects of the reconstruction inefficiency are included in the PYTHIA+DATA reference analysis.

Finally, the rate of calorimeter jets reconstructed from fluctuations in the underlying event without the presence of a fragmenting p_T parton, so called fake jets, for the jet selection used in this paper was determined using fully simulated 0–10% central HYDJET events. Reconstructed jets in this sample are classified as fake jets if no matching generator-level jet of $p_T > 20$ GeV/c

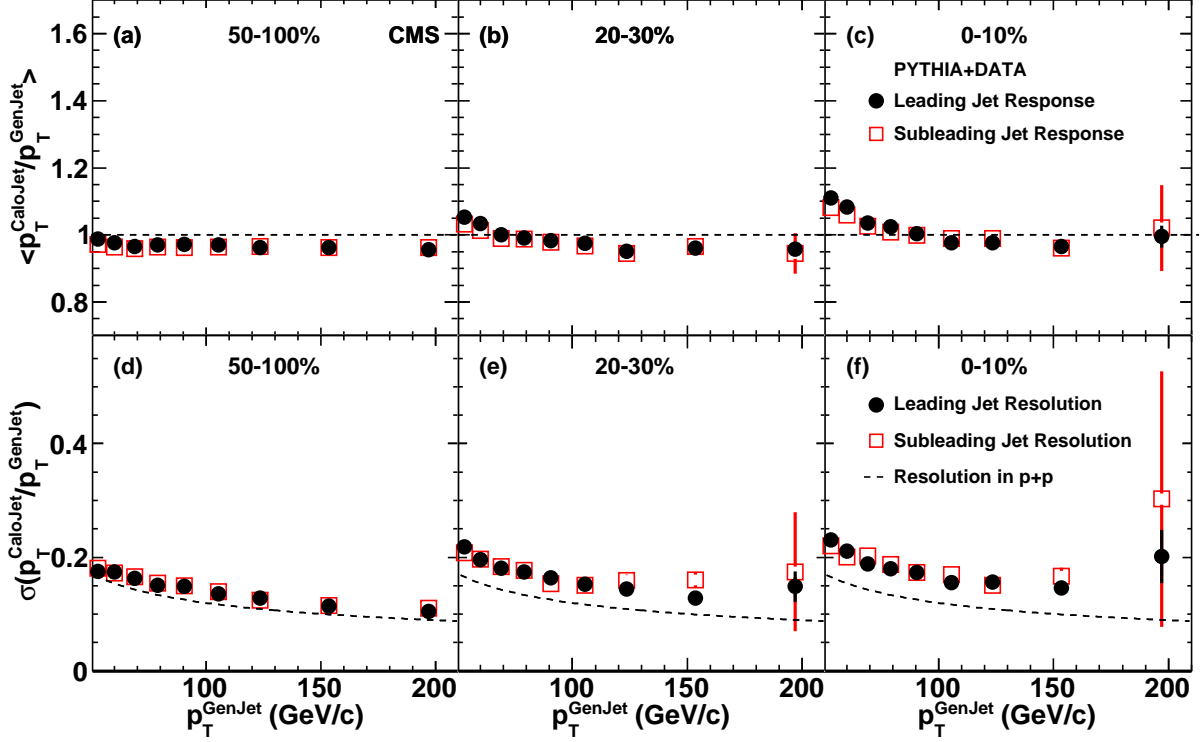


Figure 4: The top row shows the mean of the ratio of reconstructed to generated jet momenta, $\langle p_T^{\text{CaloJet}}/p_T^{\text{GenJet}} \rangle$, as a function of p_T^{GenJet} , while the bottom row shows the relative resolution, i.e., the standard deviation of $p_T^{\text{CaloJet}}/p_T^{\text{GenJet}}$. The standard pp jet energy corrections are included in p_T^{CaloJet} . Filled circles are for the leading jets and open squares are for the subleading jets. The left, center, and right columns are for jets in PYTHIA+DATA events with centrality 50–100%, 20–30%, and 0–10%, respectively. On the jet resolution plots (bottom row), the dashed line is a fit to the leading jet resolution in pp events. The vertical bars denote the statistical uncertainty.

is found within an η - ϕ distance to the reconstructed jet axis smaller than 0.3. For leading jets with $p_{T,1} > 120$ GeV/c, a fake jet fraction of less than 0.02% is found. In events with a $p_{T,1} > 120$ GeV/c leading jet, the fake jet fraction on the away-side of the leading jet ($\Delta\phi_{12} > 2\pi/3$) is determined to be 3.5% for reconstructed jets with $p_{T,2} > 50$ GeV/c and less than 0.02% for $p_{T,2} > 120$ GeV/c. The effects of the degradation of jet performance in terms of energy scale, resolution, efficiency, and fake rate on the dijet observables are discussed in Section 3.1.

3 Results

The goal of this analysis is to characterize possible modifications of dijet properties as a function of centrality in PbPb collisions. In addition to the standard event selection of inelastic hadronic collisions and the requirement of a leading jet with $p_{T,1} > 120$ GeV/c (Section 2.2), most of the subsequent analysis required the subleading jet in the event to have $p_{T,2} > 50$ GeV/c, and the azimuthal angle between the leading and subleading jet ($\Delta\phi_{12}$) to be larger than $2\pi/3$. Only jets within $|\eta| < 2$ were considered for the analysis of calorimeter jets in Section 3.1. For a data set of $L_{\text{int}} = 6.7 \mu\text{b}^{-1}$, this selection yields 3514 jet pairs. For studies of correlations of calorimeter jets with charged particles (Sections 3.2 and 3.3), a more restrictive pseudorapidity

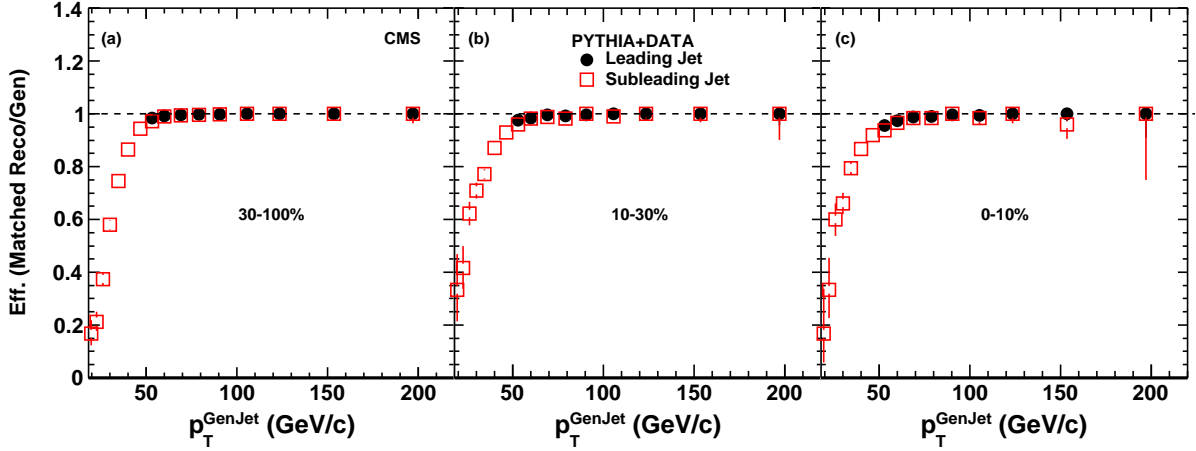


Figure 5: Jet reconstruction efficiency as a function of generator level jet p_T for the leading jet (filled circles) and subleading jet (open squares). From left to right three centrality bins are shown: 30–100%, 10–30%, 0–10%. The vertical bars denote the statistical uncertainty.

selection was applied. The analysis was performed mostly in five bins of collision centrality: 0–10%, 10–20%, 20–30%, 30–50%, and 50–100%.

Thus far, no pp reference data exist at the PbPb collision energy of $\sqrt{s_{NN}} = 2.76$ TeV. Throughout the paper, the results obtained from PbPb data will be compared to references based on the PYTHIA and PYTHIA+DATA samples described in Section 2.4.2.

For most results, the PYTHIA+DATA events will be used for direct comparisons. To calibrate the performance of PYTHIA for the observables used in this analysis, the dijet analysis was also performed using the anti- k_T algorithm on 35 pb^{-1} of pp data at $\sqrt{s} = 7$ TeV, collected by CMS prior to the heavy ion data taking and compared to PYTHIA simulations for the same collision system and energy. The same jet selection criteria used for the 2.76 TeV PbPb data were applied to both pp data and PYTHIA.

3.1 Dijet properties in pp and PbPb data

The correlation between the transverse momentum of the reconstructed leading and subleading jets in the calorimeters is plotted in Fig. 6. The top row contains PbPb data for peripheral, mid-central, and central events, the second row shows pp jets simulated by PYTHIA and embedded into PbPb data, and the bottom panel shows pp jets from PYTHIA without embedding. One can already observe a downward shift in the subleading jet p_T for the more central PbPb events. In the following discussion, a more quantitative and detailed assessment of this phenomenon will be presented.

3.1.1 Leading jet spectra

Figure 7 (a) shows the leading jet p_T distributions for 7 TeV pp data and corresponding PYTHIA simulations. The distribution of leading jet p_T for PbPb is shown in Figs. 7 (b)-(f) for five different centrality bins. The spectra obtained for PbPb data are shown as solid markers, whereas the hatched histograms show the leading jet spectrum reconstructed from PYTHIA+DATA dijet events. All spectra have been normalized to unity. The detector-level leading jet spectra in PbPb data and the corresponding results for PYTHIA+DATA samples show good quantitative agreement in all centrality bins over the p_T range studied.

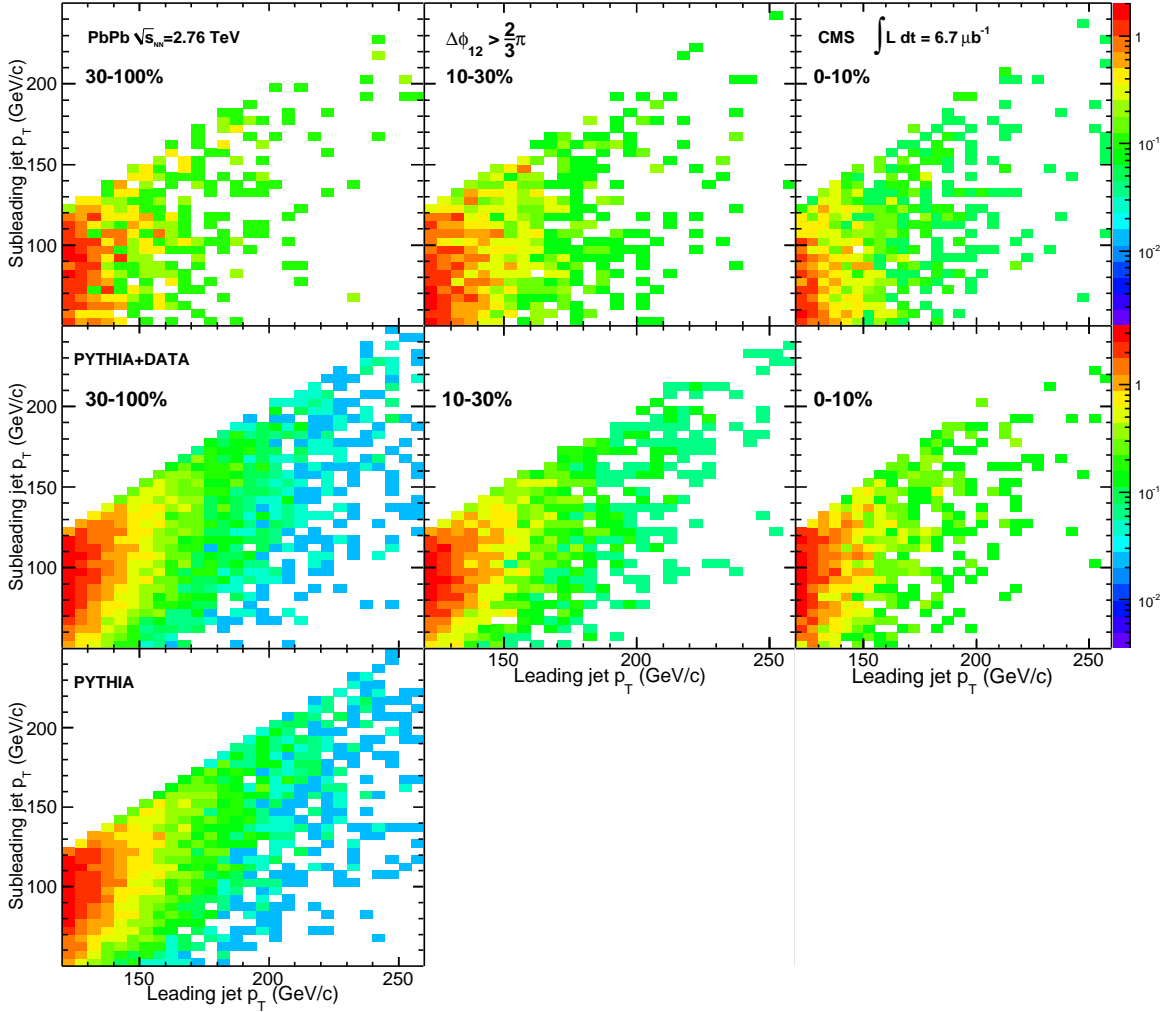


Figure 6: Subleading jet p_T vs. leading jet p_T distributions. The top two rows show results for centrality 30–100% (left column), 10–30% (middle column) and 0–10% (right column), for PbPb data (top row) and reconstructed PYTHIA jets embedded into PbPb data events (middle row). The panel in the bottom row shows the distribution for reconstructed jets from PYTHIA alone.

It is important to note that the jet momentum spectra at detector level presented here have not been corrected for smearing due to detector resolution, fluctuations in/out of the jet cone, or underlying event fluctuations. Therefore, a direct comparison of these spectra to analytical calculations or particle-level generator results is not possible. For the jet asymmetry and dijet $\Delta\phi$ distributions discussed below, the effect of the finite jet energy resolution is estimated using the PYTHIA+DATA events.

3.1.2 Dijet azimuthal correlations

One possible medium effect on the dijet properties is a change of the back-to-back alignment of the two partons. This can be studied using the event-normalized differential dijet distribution, $(1/N)(dN/d\Delta\phi_{12})$, versus $\Delta\phi_{12}$. Figure 8 shows distributions of $\Delta\phi_{12}$ between leading and subleading jets which pass the respective p_T selections. In Fig. 8 (a), the dijet $\Delta\phi_{12}$ distributions are plotted for 7 TeV pp data in comparison to the corresponding PYTHIA simulations using the anti- k_T algorithm for jets based on calorimeter information. PYTHIA provides a good de-

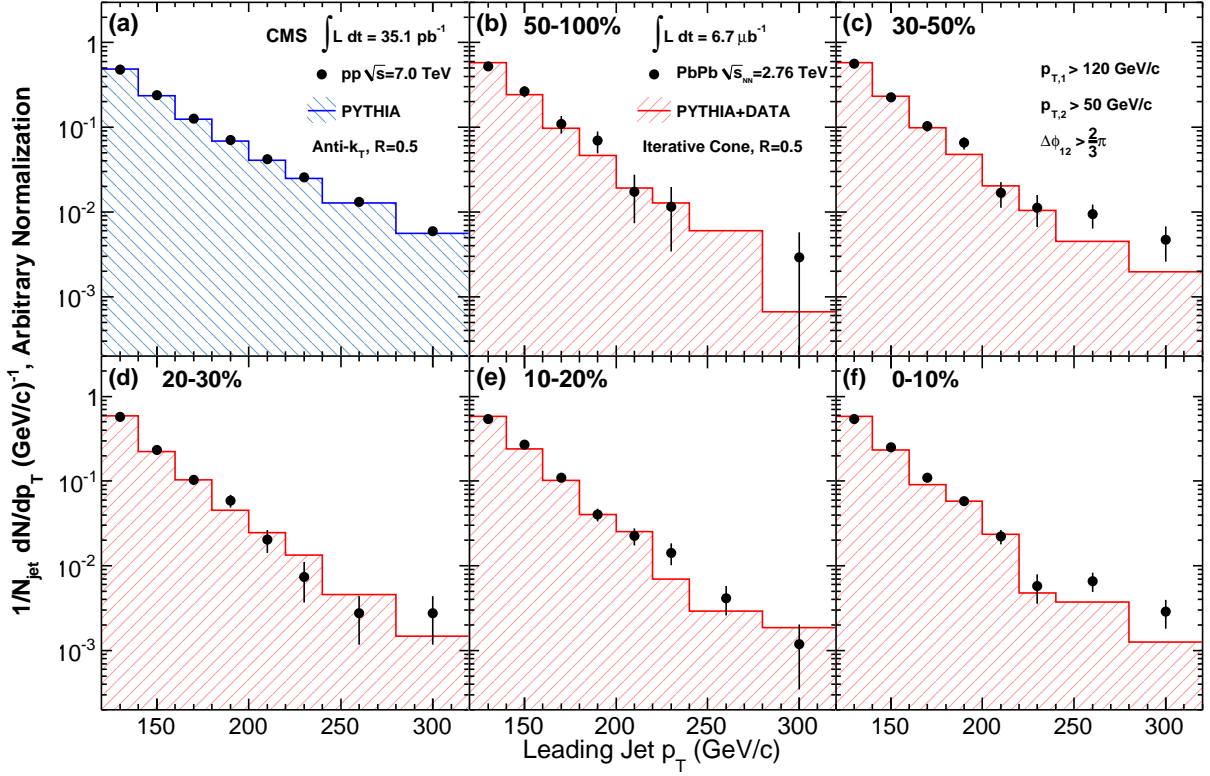


Figure 7: Leading jet p_T distribution for dijet events with subleading jets of $p_{T,2} > 50$ GeV/c and $\Delta\phi_{12} > 2\pi/3$ for 7 TeV pp collisions (a) and 2.76 TeV PbPb collisions in several centrality bins: (b) 50–100%, (c) 30–50%, (d) 20–30%, (e) 10–20% and (f) 0–10%. Data are shown as black points, while the histograms show (a) PYTHIA events and (b)–(f) PYTHIA events embedded into PbPb data. The error bars show the statistical uncertainties.

scription of the experimental data, with slightly larger tails seen in the PYTHIA simulations. A recent study of azimuthal correlations in pp collisions at 7 TeV can be found in [45]. For the PYTHIA comparison to PbPb results at $\sqrt{s_{NN}} = 2.76$ TeV, this discrepancy seen in the higher energy pp comparison is included in the systematic uncertainty estimation. It is important to note that the PYTHIA simulations include events with more than two jets, which provide the main contribution to events with large momentum imbalance or $\Delta\phi_{12}$ far from π .

Figures 8 (b)–(f) show the dijet $\Delta\phi_{12}$ distributions for PbPb data in five centrality bins, compared to PYTHIA+DATA simulations. The distributions for the four more peripheral bins are in good agreement with the PYTHIA+DATA reference, especially for $\Delta\phi_{12} \gtrsim 2$. The three centrality bins spanning 0–30% show an excess of events with azimuthally misaligned dijets ($\Delta\phi_{12} \lesssim 2$), compared with more peripheral events. A similar trend is seen for the PYTHIA+DATA simulations, although the fraction of events with azimuthally misaligned dijets is smaller in the simulation. The centrality dependence of the azimuthal correlation in PYTHIA+DATA can be understood as the result of the increasing fake-jet rate and the drop in jet reconstruction efficiency near the 50 GeV/c threshold from 95% for peripheral events to 88% for the most central events. In PbPb data, this effect is magnified since low- p_T away-side jets can undergo a sufficiently large energy loss to fall below the 50 GeV/c selection criteria.

Furthermore, a reduction of the fraction of back-to-back jets above $\Delta\phi_{12} \gtrsim 3$ is observed for the most central bin. This modification of the $\Delta\phi_{12}$ distribution as a function of centrality can be quantified using the fraction R_B of dijets with $\Delta\phi_{12} > 3.026$, as plotted in Fig. 9, for $p_{T,1} >$

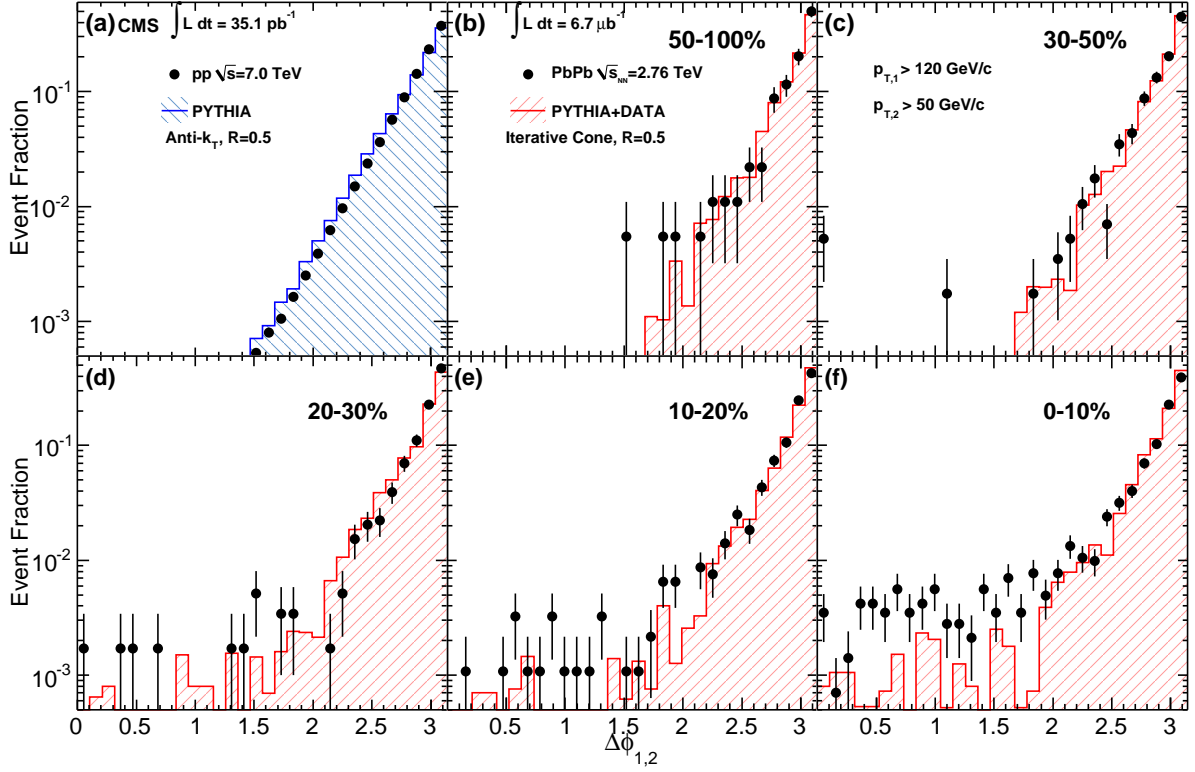


Figure 8: $\Delta\phi_{12}$ distributions for leading jets of $p_{T,1} > 120$ GeV/c with subleading jets of $p_{T,2} > 50$ GeV/c for 7 TeV pp collisions (a) and 2.76 TeV PbPb collisions in several centrality bins: (b) 50–100%, (c) 30–50%, (d) 20–30%, (e) 10–20% and (f) 0–10%. Data are shown as black points, while the histograms show (a) PYTHIA events and (b)–(f) PYTHIA events embedded into PbPb data. The error bars show the statistical uncertainties.

120 GeV/c and $p_{T,2} > 50$ GeV/c. The threshold of 3.026 corresponds to the median of the $\Delta\phi_{12}$ distribution for PYTHIA (without embedding). The results for both the PbPb data and PYTHIA+DATA dijets are shown as a function of the reaction centrality, given by the number of participating nucleons, N_{part} , as described in Section 2.3. This observable is not sensitive to the shape of the tail at $\Delta\phi_{12} < 2$ seen in Fig. 8, but can be used to measure small changes in the back-to-back correlation between dijets. A decrease in the fraction of back-to-back jets in PbPb data is seen compared to the pure PYTHIA simulations. Part of the observed change in $R_B(\Delta\phi)$ with centrality is explained by the decrease in jet azimuthal angle resolution from $\sigma_\phi = 0.03$ in peripheral events to $\sigma_\phi = 0.04$ in central events, due to the impact of fluctuations in the PbPb underlying event. This effect is demonstrated by the comparison of PYTHIA and PYTHIA+DATA results. The difference between the pp and PYTHIA+DATA resolutions was used for the uncertainty estimate, giving the dominant contribution to the systematic uncertainties, shown as brackets in Fig. 9.

3.1.3 Dijet momentum balance

To characterize the dijet momentum balance (or imbalance) quantitatively, we use the asymmetry ratio,

$$A_J = \frac{p_{T,1} - p_{T,2}}{p_{T,1} + p_{T,2}}, \quad (1)$$

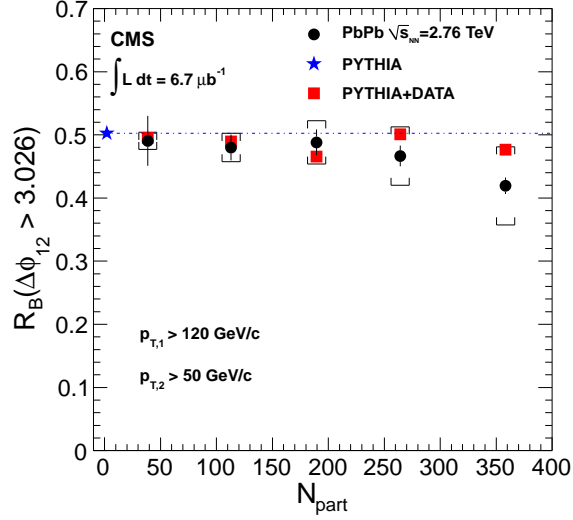


Figure 9: Fraction of events with $\Delta\phi_{12} > 3.026$ as a function of N_{part} , among events with $p_{T,1} > 120$ GeV/c and $p_{T,2} > 50$ GeV/c. The result for reconstructed PYTHIA dijet events (blue filled star) is plotted at $N_{\text{part}} = 2$. The other points (from left to right) correspond to centrality bins of 50–100%, 30–50%, 20–30%, 10–20%, and 0–10%. The red squares are for reconstruction of PYTHIA+DATA events and the filled circles are for the PbPb data, with statistical (vertical bars) and systematic (brackets) uncertainties.

where the subscript 1 always refers to the leading jet, so that A_J is positive by construction. The use of A_J removes uncertainties due to possible constant shifts of the jet energy scale. It is important to note that the subleading jet $p_{T,2} > 50$ GeV/c selection imposes a $p_{T,1}$ -dependent limit on the magnitude of A_J . For example, for the most frequent leading jets near the 120 GeV/c threshold, this limit is $A_J < 0.41$, while the largest possible A_J for the present dataset is 0.7 for 300 GeV/c leading jets. Dijets in which the subleading jet is lost below the 50 GeV/c threshold are not included in the A_J calculation.

In Fig. 10 (a), the A_J dijet asymmetry observable calculated by PYTHIA is compared to pp data at $\sqrt{s} = 7$ TeV. Again, data and event generator are found to be in excellent agreement. This observation, as well as the good agreement between PYTHIA+DATA and the most peripheral PbPb data shown in Fig. 10 (b), suggests that PYTHIA at $\sqrt{s} = 2.76$ TeV can serve as a good reference for the dijet imbalance analysis in PbPb collisions.

The centrality dependence of A_J for PbPb collisions can be seen in Figs. 10 (b)-(f), in comparison to PYTHIA+DATA simulations. Whereas the dijet angular correlations show only a small dependence on collision centrality, the dijet momentum balance exhibits a dramatic change in shape for the most central collisions. In contrast, the PYTHIA simulations only exhibit a modest broadening, even when embedded in the highest multiplicity PbPb events.

Central PbPb events show a significant deficit of events in which the momenta of leading and subleading jets are balanced and a significant excess of unbalanced pairs. The large excess of unbalanced compared to balanced dijets explains why this effect was apparent even when simply scanning event displays (see Fig. 1). The striking momentum imbalance is also confirmed when studying high- p_T tracks associated with leading and subleading jets, as will be shown in Section 3.2. It is consistent with a degradation of the parton energy, or jet quenching, in the medium produced in central PbPb collisions.

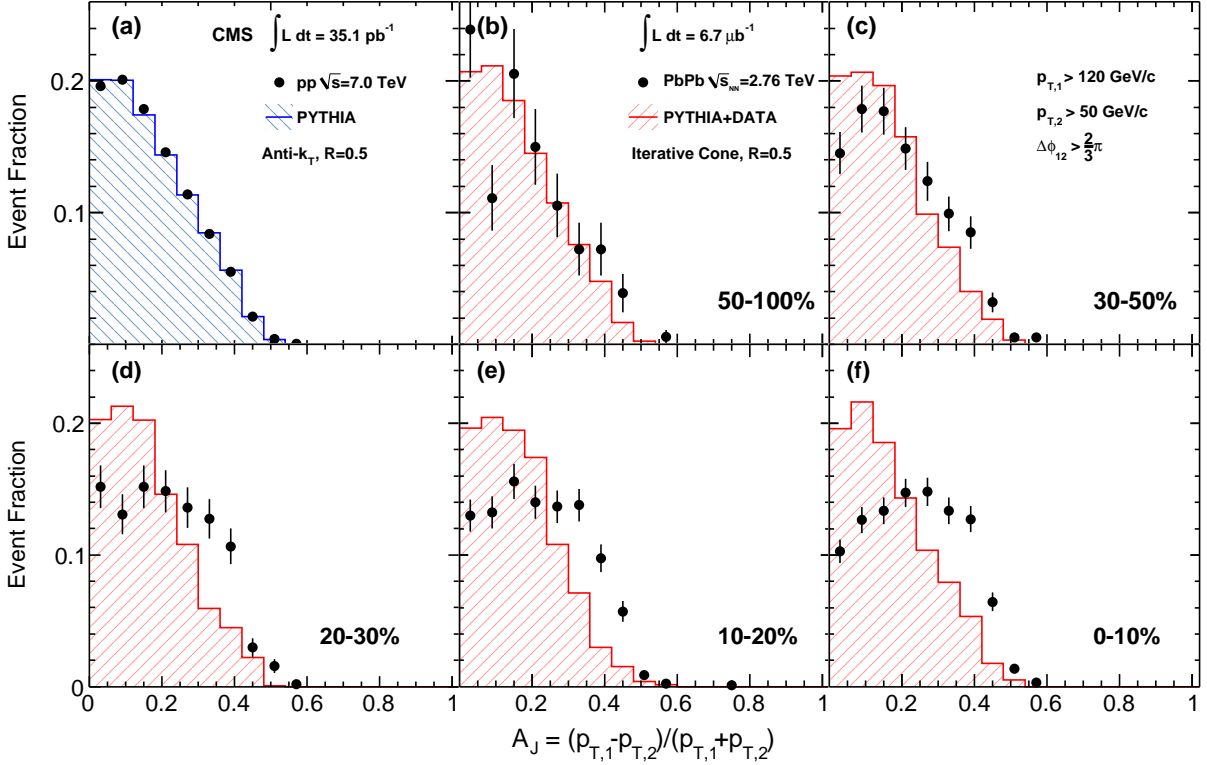


Figure 10: Dijet asymmetry ratio, A_J , for leading jets of $p_{T,1} > 120 \text{ GeV}/c$, subleading jets of $p_{T,2} > 50 \text{ GeV}/c$ and $\Delta\phi_{12} > 2\pi/3$ for 7 TeV pp collisions (a) and 2.76 TeV PbPb collisions in several centrality bins: (b) 50–100%, (c) 30–50%, (d) 20–30%, (e) 10–20% and (f) 0–10%. Data are shown as black points, while the histograms show (a) PYTHIA events and (b)–(f) PYTHIA events embedded into PbPb data. The error bars show the statistical uncertainties.

The evolution of the dijet momentum balance illustrated in Fig. 10 can be explored more quantitatively by studying the fraction of balanced jets in the PbPb events. The balanced fraction, $R_B(A_J < 0.15)$, is plotted as a function of collision centrality (again in terms of N_{part}) in Fig. 11. It is defined as the fraction of all events with a leading jet having $p_{T,1} > 120 \text{ GeV}/c$ for which a subleading partner with $A_J < 0.15$ and $\Delta\phi_{12} > 2\pi/3$ is found. Since $R_B(A_J < 0.15)$ is calculated as the fraction of all events with $p_{T,1} > 120 \text{ GeV}/c$, it takes into account the rate of apparent “mono-jet” events, where the subleading partner is removed by the p_T or $\Delta\phi$ selection.

The A_J threshold of 0.15 corresponds to the median of the A_J distribution for pure PYTHIA dijet events passing the criteria used for Fig. 10. By definition, the fraction $R_B(A_J < 0.15)$ of balanced jets in PYTHIA is therefore 50%, which is plotted as a dashed line in Fig. 11. As will be discussed in Section 3.3, a third jet having a significant impact on the dijet imbalance is present in most of the large- A_J events in PYTHIA.

The change in jet-finding performance from high to low p_T , discussed in Section 2.4.3, leads to only a small decrease in the fraction of balanced jets, of less than 5% for central PYTHIA+DATA dijets. In contrast, the PbPb data show a rapid decrease in the fraction of balanced jets with collision centrality. While the most peripheral selection shows a fraction of balanced jets of close to 45%, this fraction drops by close to a factor of two for the most central collisions. This again suggests that the passage of hard-scattered partons through the environment created in PbPb collisions has a significant impact on their fragmentation into final-state jets.

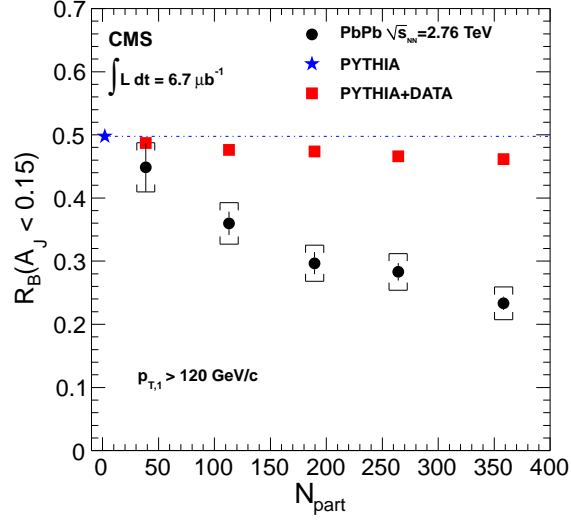


Figure 11: Fraction of all events with a leading jet with $p_{T,1} > 120$ GeV/c for which a subleading jet with $A_J < 0.15$ and $\Delta\phi_{12} > 2\pi/3$ was found, as a function of N_{part} . The result for reconstructed PYTHIA dijet events (blue filled star) is plotted at $N_{part} = 2$. The other points (from left to right) correspond to centrality bins of 50–100%, 30–50%, 20–30%, 10–20%, and 0–10%. The red squares are for reconstruction of PYTHIA+DATA events and the filled circles are for the PbPb data, with statistical (vertical bars) and systematic (brackets) uncertainties.

The observed change in the fraction of balanced jets as a function of centrality, shown in Fig. 11, is far bigger than the estimated systematic uncertainties, shown as brackets. The main contributions to the systematic uncertainties include the uncertainties on jet energy scale and resolution, jet reconstruction efficiency, and the effects of underlying event subtraction. The uncertainty in the subtraction procedure is estimated based on the difference between pure PYTHIA and PYTHIA+DATA simulations. For central events, the subtraction procedure contributes the biggest uncertainty to $R_B(A_J)$, of close to 8%. The uncertainty on the residual jet energy scale was estimated based on the results shown in the top row of Fig. 4. The full difference between the observed residual correction and unity, added in quadrature with the systematic uncertainty obtained for pp [34], was used as the systematic uncertainty on the jet p_T and propagated to $R_B(A_J)$. For the jet p_T resolution uncertainty, the full difference of the PYTHIA+DATA result to the pp resolution, as shown in Fig. 4 (bottom), was used as an uncertainty estimate for the PbPb jet p_T resolution. The uncertainties in jet energy scale and jet resolution contribute 5% and 6%, respectively, to the 11% total systematic uncertainty in central events. For peripheral events, the total uncertainty drops to 9%, mostly due to the smaller uncertainty related to the PbPb background fluctuations for lower multiplicity events.

3.1.4 Leading jet p_T dependence of dijet momentum imbalance

The dependence of the jet modification on the leading jet momentum can be studied using the fractional imbalance $\Delta p_{T,rel} = (p_{T,1} - p_{T,2})/p_{T,1}$. The mean value of this fraction is presented as a function of $p_{T,1}$ in Fig. 12 for three bins of collision centrality, 30–100%, 10–30% and 0–10%. PYTHIA is shown as stars, PYTHIA+DATA simulations are shown as squares, while the data are shown as circles. Statistical and systematic uncertainties are plotted as error bars and brackets, respectively. The dominant contribution to the systematic uncertainty comes from the observed p_T dependence of the residual jet energy correction in PbPb events (6% out of a total systematic uncertainty of 8%). The jet energy resolution and underlying event subtraction uncertainties

contribute about 4% each.

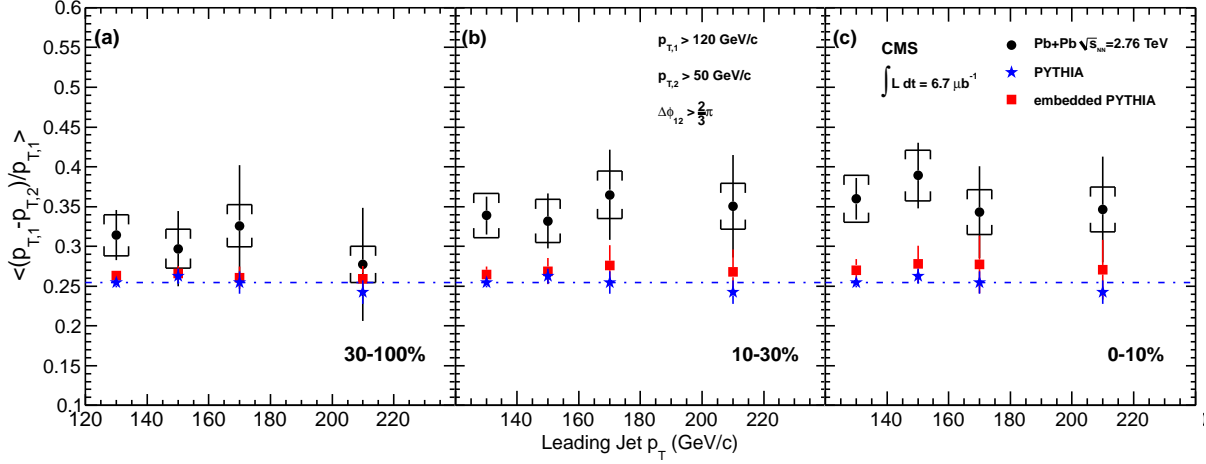


Figure 12: Mean value of the fractional imbalance $(p_{T,1} - p_{T,2})/p_{T,1}$ as a function of leading jet p_T for three centrality bins. The PbPb data are shown as circles with vertical bars and brackets indicating the statistical and systematic uncertainties, respectively. Results for PYTHIA are shown with blue stars, and PYTHIA+DATA with red squares. The dot-dashed line to guide the eye is drawn at the value for pure PYTHIA for the lowest p_T bin.

The fractional imbalance exhibits several important features: the imbalance seen in PbPb data grows with collision centrality and reaches a much larger value than in PYTHIA or PYTHIA+DATA. In addition, the effect is clearly visible even for the highest- p_T jets observed in the data set, demonstrating that the observed dijet imbalance is not restricted to the threshold region in our leading jet selection. Within the present uncertainties, the $p_{T,1}$ dependence of the excess imbalance above the PYTHIA prediction is compatible with either a constant difference or a constant fraction of $p_{T,1}$.

The main contributions to the systematic uncertainty in $(p_{T,1} - p_{T,2})/p_{T,1}$ are the uncertainties in the p_T -dependent residual energy scale (based on results shown in the top row of Fig. 4), and the centrality-dependent difference observed between PYTHIA and PYTHIA+DATA seen in Fig. 12. As before, the uncertainty on the residual jet energy scale was estimated using the full difference between the observed residual correction and unity, and also assuming that within these limits the low- p_T and high- p_T response could vary independently.

3.2 Track-jet correlations

The studies of calorimeter jets show a strong change of the jet momentum balance as a function of collision centrality. This implies a corresponding modification in the distribution of jet fragmentation products, with energy being either transported out of the cone area used to define the jets, or to low-momentum particles which are not measured in the calorimeter jets. The CMS calorimeter is less sensitive to these low momentum particles, or they do not reach the calorimeter surface. Information about changes to the effective fragmentation pattern as a function of A_J can be obtained from track-jet correlations. For this analysis, PYTHIA+HYDJET simulations are used as MC reference, to allow full access to MC truth (i.e., the output of the generator) information for tracks in the dijet signal and in the PbPb underlying event. The event selection for PYTHIA+HYDJET was based on reconstructed calorimeter jet information, as for the previous studies.

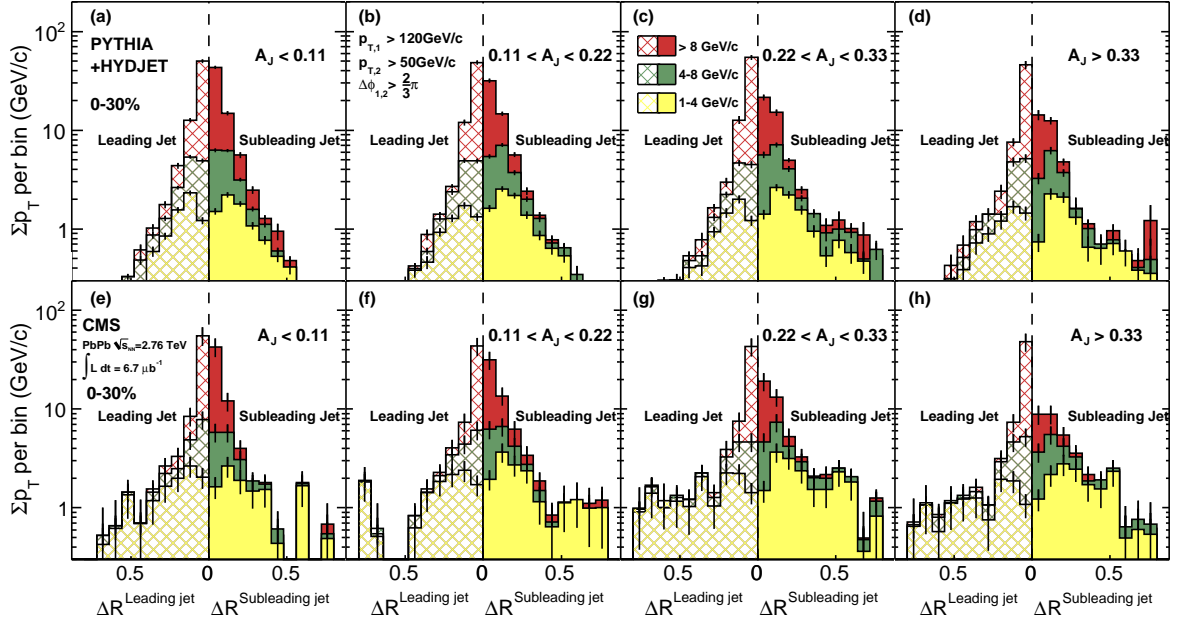


Figure 13: Distribution of the transverse momentum sum of tracks for three p_T ranges, as a function of the distance ΔR to the leading and subleading jet axes. Results for the 0–30% centrality selection are shown for PYTHIA+HYDJET (upper row) and PbPb data (lower row). For each figure, the requirements on the dijet asymmetry A_J are given. Note that events with $A_J > 0.22$ are much rarer in the PYTHIA+HYDJET sample than in the data. Vertical bars are statistical and systematic uncertainties, combined in quadrature, the systematic contributions being 20%, independent of the bin.

To derive the associated track spectrum for a given jet selection in data, the p_T distribution of tracks inside a ring of radius $\Delta R = \sqrt{\Delta\phi^2 + \Delta\eta^2}$ and width of 0.08 around the jet axes was summed over all selected jets. The contribution of tracks from the underlying event, not associated with the jet, was estimated by summing the track p_T distributions using an equal-size ring that was reflected around $\eta = 0$, but at the same ϕ coordinate as the individual jet. For this procedure, jets in the region $|\eta| < 0.8$ were excluded and only ring-radii up to $\Delta R = 0.8$ around the jet axes were considered, to avoid overlap between the signal jet region and the region used for background estimation. In addition, jets in the region $|\eta| > 1.6$ were excluded to ensure the 0.8 radius rings would lie within the tracker acceptance. Statistical fluctuations in the underlying event limit this procedure to tracks with transverse momenta $p_T > 1$ GeV/c.

The summed p_T spectra from the jet regions and the underlying event regions were then subtracted, yielding the momentum distribution of charged tracks associated with the jets as a function of ΔR .

The resulting distributions of associated track momentum as a function of track p_T and ΔR are presented in Fig. 13 for four selections in dijet asymmetry, from $A_J < 0.11$ (left) to $A_J > 0.33$ (right). For both data and PYTHIA+HYDJET results, the jet selections and A_J values are based on the reconstructed calorimeter jet momenta (Section 2.4) in order to have consistent event selections for comparison. The middle bin boundary ($A_J = 0.22$) corresponds to the median of the A_J distribution for the 0–30% central PbPb events shown here. The top row shows the results for PYTHIA+HYDJET simulations. The track results shown for the PYTHIA+HYDJET simulations were found using the known (“truth”) values of the track momenta from the embedded PYTHIA events. The bottom row presents results for PbPb data. The track results shown for PbPb data

were corrected for tracking efficiency and fake rates using corrections that were derived from PYTHIA+HYDJET simulations and from the reconstruction of single tracks embedded in data. In each panel, the area of each colored region in p_T and ΔR corresponds to the total transverse momentum per event carried by tracks in this region.

For the balanced-jet selection, $A_J < 0.11$, one sees qualitative agreement in the leading and subleading jet momentum distributions between PYTHIA+HYDJET (top) and data (bottom). In data and simulation, most of the leading and subleading jet momentum is carried by tracks with $p_T > 8$ GeV/c, with the data tracks having a slightly narrower ΔR distribution. A slightly larger fraction of the momentum for the subleading jets is carried by tracks at low p_T and $\Delta R > 0.16$ (i.e., beyond the second bin) in the data.

Moving towards larger dijet imbalance, the major fraction of the leading jet momentum continues to be carried by high- p_T tracks in data and simulation. For the $A_J > 0.33$ selection, it is important to recall that less than 10% of all PYTHIA dijet events fall in this category, and, as will be discussed in Section 3.3, those that do are overwhelmingly 3-jet events.

While the overall change found in the leading jet shapes as a function of A_J is small, a strong modification of the track momentum composition of the subleading jets is seen, confirming the calorimeter determination of the dijet imbalance. The biggest difference between data and simulation is found for tracks with $p_T < 4$ GeV/c. For PYTHIA, the momentum in the subleading jet carried by these tracks is small and their radial distribution is nearly unchanged with A_J . However, for data, the relative contribution of low- p_T tracks grows with A_J , and an increasing fraction of those tracks is observed at large distances to the jet axis, extending out to $\Delta R = 0.8$ (the largest angular distance to the jet in this study).

The major systematic uncertainties for the track-jet correlation measurement come from the p_T -dependent uncertainty in the track reconstruction efficiency. The algorithmic track reconstruction efficiency, which averages 70% over the $p_T > 0.5$ GeV/c and $|\eta| < 2.4$ range included in this study, was determined from an independent PYTHIA+HYDJET sample, and from simulated tracks embedded in data. Additional uncertainties are introduced by the underlying event subtraction procedure. The latter was studied by comparing the track-jet correlations seen in pure PYTHIA dijet events for generated particles with those seen in PYTHIA+HYDJET events after reconstruction and background subtraction. The size of the background subtraction systematic uncertainty was further cross-checked in data by repeating the procedure for random ring-like regions in 0–30% central minimum bias events. In the end, an overall systematic uncertainty of 20% per bin was assigned. This uncertainty is included in the combined statistical and systematic uncertainties shown in Fig. 13.

3.3 Overall momentum balance of dijet events

The requirements of the background subtraction procedure limit the track-jet correlation study to tracks with $p_T > 1.0$ GeV/c and $\Delta R < 0.8$. Complementary information about the overall momentum balance in the dijet events can be obtained using the projection of missing p_T of reconstructed charged tracks onto the leading jet axis. For each event, this projection was calculated as

$$p_T^{\parallel} = \sum_i -p_T^i \cos(\phi_i - \phi_{\text{Leading Jet}}), \quad (2)$$

where the sum is over all tracks with $p_T > 0.5$ GeV/c and $|\eta| < 2.4$. The results were then averaged over events to obtain $\langle p_T^{\parallel} \rangle$. No background subtraction was applied, which allows

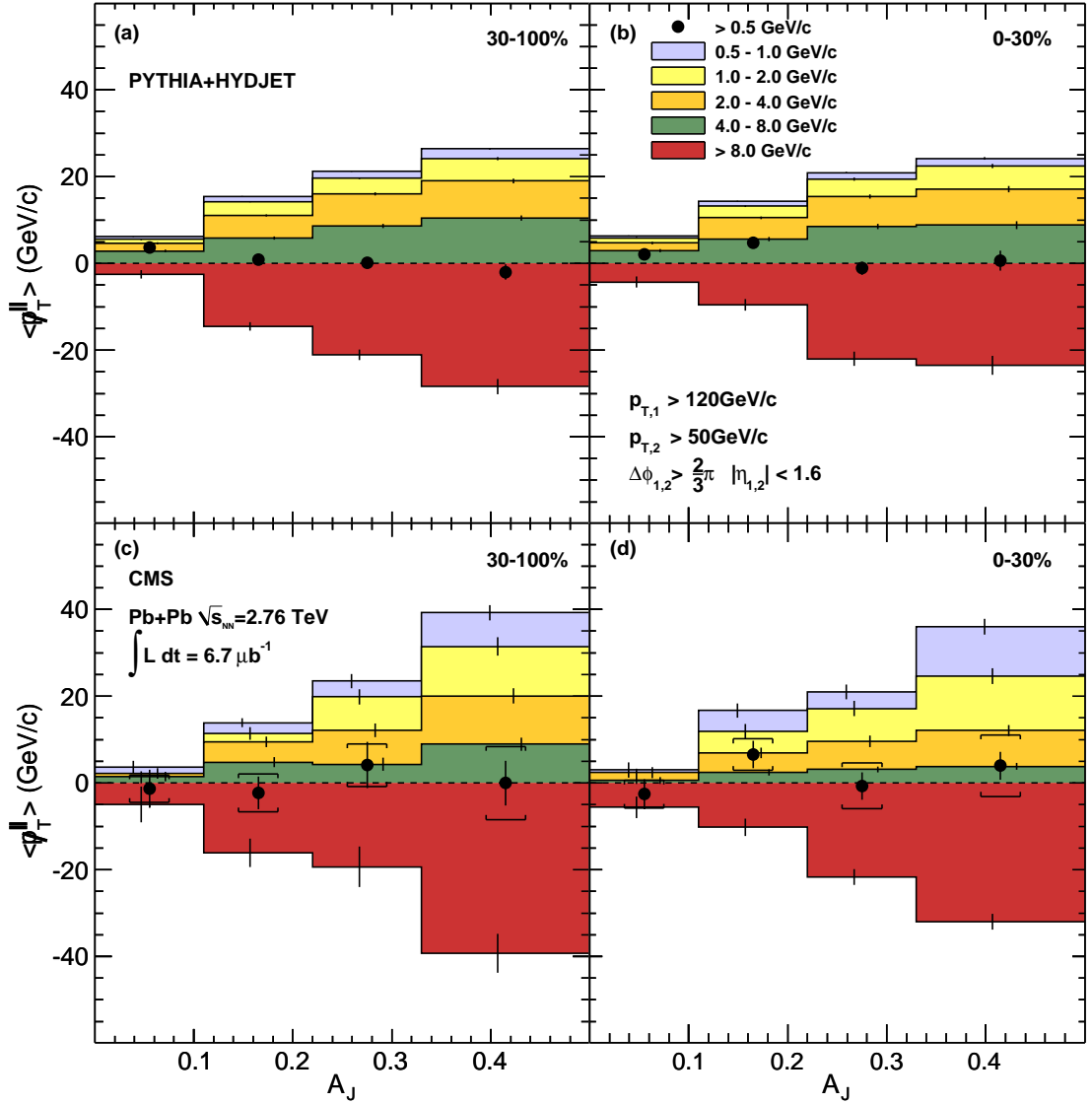


Figure 14: Average missing transverse momentum, $\langle p_T^{\parallel} \rangle$, for tracks with $p_T > 0.5$ GeV/c, projected onto the leading jet axis (solid circles). The $\langle p_T^{\parallel} \rangle$ values are shown as a function of dijet asymmetry A_J for 30–100% centrality (left) and 0–30% centrality (right). For the solid circles, vertical bars and brackets represent the statistical and systematic uncertainties, respectively. Colored bands show the contribution to $\langle p_T^{\parallel} \rangle$ for five ranges of track p_T . The top and bottom rows show results for PYTHIA+HYDJET and PbPb data, respectively. For the individual p_T ranges, the statistical uncertainties are shown as vertical bars.

this study to include the $|\eta_{jet}| < 0.8$ and $0.5 < p_T^{\text{Track}} < 1.0$ GeV/c regions not accessible for the study in Section 3.2. The leading and subleading jets were again required to have $|\eta| < 1.6$.

In Fig. 14, $\langle p_T^{\parallel} \rangle$ is shown as a function of A_J for two centrality bins, 30–100% (left) and 0–30% (right). Results for PYTHIA+HYDJET are presented in the top row, while the bottom row shows the results for PbPb data. Using tracks with $|\eta| < 2.4$ and $p_T > 0.5$ GeV/c, one sees that indeed the momentum balance of the events, shown as solid circles, is recovered within uncertainties,

for both centrality ranges and even for events with large observed dijet asymmetry, in both data and simulation. This shows that the dijet momentum imbalance is not related to undetected activity in the event due to instrumental (e.g. gaps or inefficiencies in the calorimeter) or physics (e.g. neutrino production) effects.

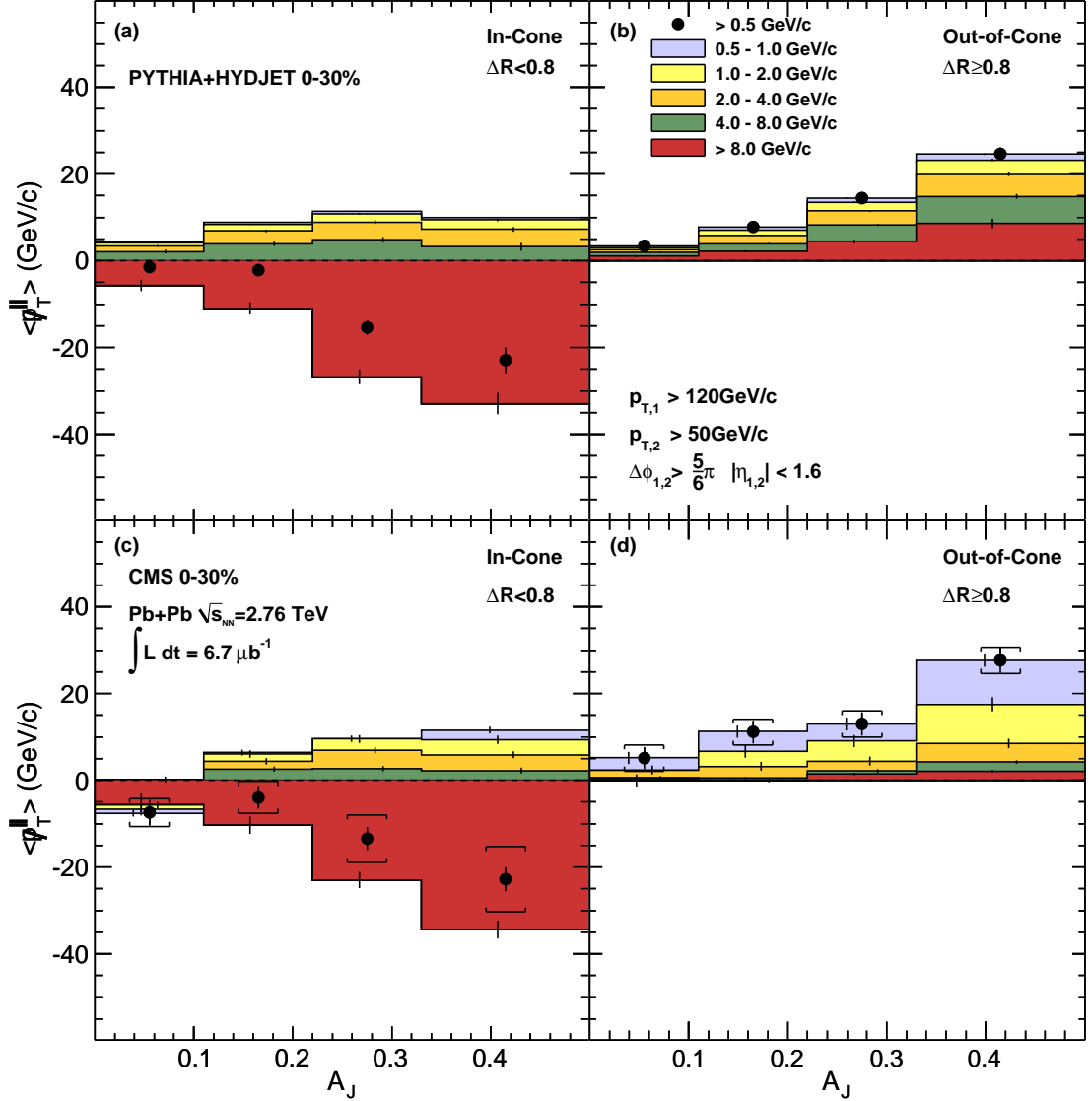


Figure 15: Average missing transverse momentum, $\langle p_T^{\parallel} \rangle$, for tracks with $p_T > 0.5 \text{ GeV}/c$, projected onto the leading jet axis (solid circles). The $\langle p_T^{\parallel} \rangle$ values are shown as a function of dijet asymmetry A_J for 0–30% centrality, inside ($\Delta R < 0.8$) one of the leading or subleading jet cones (left) and outside ($\Delta R > 0.8$) the leading and subleading jet cones (right). For the solid circles, vertical bars and brackets represent the statistical and systematic uncertainties, respectively. For the individual p_T ranges, the statistical uncertainties are shown as vertical bars.

The figure also shows the contributions to $\langle p_T^{\parallel} \rangle$ for five transverse momentum ranges from 0.5–1 GeV/c to $p_T > 8 \text{ GeV}/c$. The vertical bars for each range denote statistical uncertainties. For data and simulation, a large negative contribution to $\langle p_T^{\parallel} \rangle$ (i.e., in the direction of the leading jet)

by the $p_T > 8$ GeV/ c range is balanced by the combined contributions from the 0.5–8 GeV/ c regions. Looking at the $p_T < 8$ GeV/ c region in detail, important differences between data and simulation emerge. For PYTHIA+HYDJET both centrality ranges show a large balancing contribution from the intermediate p_T region of 4–8 GeV/ c , while the contribution from the two regions spanning 0.5–2 GeV/ c is very small. In peripheral PbPb data, the contribution of 0.5–2 GeV/ c tracks relative to that from 4–8 GeV/ c tracks is somewhat enhanced compared to the simulation. In central PbPb events, the relative contribution of low and intermediate- p_T tracks is actually the opposite of that seen in PYTHIA+HYDJET. In data, the 4–8 GeV/ c region makes almost no contribution to the overall momentum balance, while a large fraction of the negative imbalance from high p_T is recovered in low-momentum tracks.

The dominant systematic uncertainty for the p_T balance measurement comes from the p_T -dependent uncertainty in the track reconstruction efficiency and fake rate described in Section 3.2. A 20% uncertainty was assigned to the final result, stemming from the residual difference between the PYTHIA generator-level and the reconstructed PYTHIA+HYDJET tracks at high p_T . This is combined with an absolute 3 GeV/ c uncertainty that comes from the imperfect cancellation of the background tracks. The background effect was cross-checked in data from a random cone study in 0–30% central events similar to the study described in Section 3.2. The overall systematic uncertainty is shown as brackets in Figs. 14 and 15.

Further insight into the radial dependence of the momentum balance can be gained by studying $\langle p_T^\parallel \rangle$ separately for tracks inside cones of size $\Delta R = 0.8$ around the leading and subleading jet axes, and for tracks outside of these cones. The results of this study for central events are shown in Fig. 15 for the in-cone balance and out-of-cone balance for MC and data. As the underlying PbPb event in both data and MC is not ϕ -symmetric on an event-by-event basis, the back-to-back requirement was tightened to $\Delta\phi_{12} > 5\pi/6$ for this study.

One observes that for both data and MC an in-cone imbalance of $\langle p_T^\parallel \rangle \approx -20$ GeV/ c is found for the $A_J > 0.33$ selection. In both cases this is balanced by a corresponding out-of-cone imbalance of $\langle p_T^\parallel \rangle \approx 20$ GeV/ c . However, in the PbPb data the out-of-cone contribution is carried almost entirely by tracks with $0.5 < p_T < 4$ GeV/ c whereas in MC more than 50% of the balance is carried by tracks with $p_T > 4$ GeV/ c , with a negligible contribution from $p_T < 1$ GeV/ c .

The PYTHIA+HYDJET results are indicative of semi-hard initial or final-state radiation as the underlying cause for large A_J events in the MC study. This has been confirmed by further studies which showed that in PYTHIA the momentum balance in the transverse plane for events with large A_J can be restored if a third jet with $p_T > 20$ GeV/ c , which is present in more than 90% of these events, is included. This is in contrast to the results for large- A_J PbPb data, which show that a large part of the momentum balance is carried by soft particles ($p_T < 2$ GeV/ c) and radiated at large angles to the jet axes ($\Delta R > 0.8$).

4 Summary

The CMS detector has been used to study jet production in PbPb collisions at $\sqrt{s_{NN}} = 2.76$ TeV. Jets were reconstructed using primarily the calorimeter information in a data sample corresponding to an integrated luminosity of $L_{\text{int}} = 6.7 \mu\text{b}^{-1}$. Events having a leading jet with $p_T > 120$ GeV/ c and $|\eta| < 2$ were selected. As a function of centrality, dijet events with a subleading jet of $p_T > 50$ GeV/ c and $|\eta| < 2$ were found to have an increasing momentum imbalance. Data were compared to PYTHIA dijet simulations for pp collisions at the same energy which were embedded into real heavy ion events. The momentum imbalances observed in the

data were significantly larger than those predicted by the simulations. While the relative imbalance between the leading and subleading jets increased with increasing collision centrality, it was found to be largely independent of the leading jet p_T , up to the highest p_T region studied (≈ 210 GeV/ c).

The angular distribution of jet fragmentation products has been explored by associating charged tracks with the dijets observed in the calorimeters. The calorimeter-based momentum imbalance is reflected in the associated track distributions, which show a softening and widening of the subleading jet fragmentation pattern for increasing dijet asymmetry, while the high- p_T components of the leading jet remain nearly unchanged.

Studies of the missing transverse momentum projected on the jet axis have shown that the overall momentum balance can be recovered if tracks at low p_T are included. In the PbPb data, but not in the simulations, a large fraction of the balancing momentum is carried by tracks having $p_T < 2$ GeV/ c . Comparing the momentum balance inside and outside of cones of $\Delta R = 0.8$ around the leading and subleading jet axes demonstrates that a large contribution to the momentum balance in data arises from soft particles radiated at $\Delta R > 0.8$ to the jets, a feature which is also not reproduced in PYTHIA calculations.

In conclusion, a strong increase in the fraction of highly unbalanced jets has been seen in central PbPb collisions compared with peripheral collisions and model calculations, consistent with a high degree of jet quenching in the produced matter. A large fraction of the momentum balance of these unbalanced jets is carried by low- p_T particles at large radial distance, in contrast to PYTHIA simulations embedded into heavy ion events. The results provide qualitative constraints on the nature of the jet modification in PbPb collisions and quantitative input to models of the transport properties of the medium created in these collisions.

Acknowledgments

We wish to congratulate our colleagues in the CERN accelerator departments for the excellent performance of the LHC machine. We thank the technical and administrative staff at CERN and other CMS institutes. This work was supported by the Austrian Federal Ministry of Science and Research; the Belgium Fonds de la Recherche Scientifique, and Fonds voor Wetenschappelijk Onderzoek; the Brazilian Funding Agencies (CNPq, CAPES, FAPERJ, and FAPESP); the Bulgarian Ministry of Education and Science; CERN; the Chinese Academy of Sciences, Ministry of Science and Technology, and National Natural Science Foundation of China; the Colombian Funding Agency (COLCIENCIAS); the Croatian Ministry of Science, Education and Sport; the Research Promotion Foundation, Cyprus; the Estonian Academy of Sciences and NICPB; the Academy of Finland, Finnish Ministry of Education, and Helsinki Institute of Physics; the Institut National de Physique Nucléaire et de Physique des Particules / CNRS, and Commissariat à l'Énergie Atomique et aux Énergies Alternatives / CEA, France; the Bundesministerium für Bildung und Forschung, Deutsche Forschungsgemeinschaft, and Helmholtz-Gemeinschaft Deutscher Forschungszentren, Germany; the General Secretariat for Research and Technology, Greece; the National Scientific Research Foundation, and National Office for Research and Technology, Hungary; the Department of Atomic Energy, and Department of Science and Technology, India; the Institute for Studies in Theoretical Physics and Mathematics, Iran; the Science Foundation, Ireland; the Istituto Nazionale di Fisica Nucleare, Italy; the Korean Ministry of Education, Science and Technology and the World Class University program of NRF, Korea; the Lithuanian Academy of Sciences; the Mexican Funding Agencies (CINVESTAV, CONACYT, SEP, and UASLP-FAI); the Pakistan Atomic Energy Commission; the State Commission for Scientific Research, Poland; the Fundação para a Ciência e a Tecnologia, Portugal; JINR

(Armenia, Belarus, Georgia, Ukraine, Uzbekistan); the Ministry of Science and Technologies of the Russian Federation, and Russian Ministry of Atomic Energy; the Ministry of Science and Technological Development of Serbia; the Ministerio de Ciencia e Innovación, and Programa Consolider-Ingenio 2010, Spain; the Swiss Funding Agencies (ETH Board, ETH Zurich, PSI, SNF, UniZH, Canton Zurich, and SER); the National Science Council, Taipei; the Scientific and Technical Research Council of Turkey, and Turkish Atomic Energy Authority; the Science and Technology Facilities Council, UK; the US Department of Energy, and the US National Science Foundation. Individuals have received support from the Marie-Curie programme and the European Research Council (European Union); the Leventis Foundation; the A. P. Sloan Foundation; the Alexander von Humboldt Foundation; the Associazione per lo Sviluppo Scientifico e Tecnologico del Piemonte (Italy); the Belgian Federal Science Policy Office; the Fonds pour la Formation à la Recherche dans l'Industrie et dans l'Agriculture (FRIA-Belgium); and the Agentschap voor Innovatie door Wetenschap en Technologie (IWT-Belgium).

References

- [1] E. V. Shuryak, "Theory of Hadronic Plasma", *Sov. Phys. JETP* **47** (1978) 212.
- [2] J. C. Collins and M. J. Perry, "Superdense Matter: Neutrons Or Asymptotically Free Quarks?", *Phys. Rev. Lett.* **34** (1975) 1353. doi:10.1103/PhysRevLett.34.1353.
- [3] N. Cabibbo and G. Parisi, "Exponential Hadronic Spectrum and Quark Liberation", *Phys. Lett.* **B59** (1975) 67. doi:10.1016/0370-2693(75)90158-6.
- [4] B. A. Freedman and L. D. McLerran, "Fermions and Gauge Vector Mesons at Finite Temperature and Density. 3. The Ground State Energy of a Relativistic Quark Gas", *Phys. Rev.* **D16** (1977) 1169. doi:10.1103/PhysRevD.16.1169.
- [5] F. Karsch and E. Laermann, "Thermodynamics and in-medium hadron properties from lattice QCD", *Quark-Gluon Plasma III, R. Hwa (ed.)* (2003) arXiv:hep-lat/0305025.
- [6] J. D. Bjorken, "Energy loss of energetic partons in QGP: possible extinction of high pT jets in hadron-hadron collisions", *FERMILAB-PUB-82-059-THY* (1982).
- [7] J. Casalderrey-Solana and C. A. Salgado, "Introductory lectures on jet quenching in heavy ion collisions", *Acta Phys. Polon.* **B38** (2007) 3731, arXiv:0712.3443.
- [8] D. d'Enterria, "Jet quenching", *Landolt-Boernstein, Springer-Verlag* **Vol. 1-23A** (2010) 99, arXiv:0902.2011.
- [9] PHENIX Collaboration, "Formation of dense partonic matter in relativistic nucleus nucleus collisions at RHIC: Experimental evaluation by the PHENIX collaboration", *Nucl. Phys.* **A757** (2005) 184, arXiv:nucl-ex/0410003. doi:10.1016/j.nuclphysa.2005.03.086.
- [10] STAR Collaboration, "Experimental and theoretical challenges in the search for the quark gluon plasma: The STAR collaboration's critical assessment of the evidence from RHIC collisions", *Nucl. Phys.* **A757** (2005) 102, arXiv:nucl-ex/0501009. doi:10.1016/j.nuclphysa.2005.03.085.
- [11] PHOBOS Collaboration, "The PHOBOS perspective on discoveries at RHIC", *Nucl. Phys.* **A757** (2005) 28, arXiv:nucl-ex/0410022. doi:10.1016/j.nuclphysa.2005.03.084.

-
- [12] BRAHMS Collaboration, "Quark Gluon Plasma and Color Glass Condensate at RHIC? The perspective from the BRAHMS experiment", *Nucl. Phys.* **A757** (2005) 1, arXiv:nucl-ex/0410020. doi:10.1016/j.nuclphysa.2005.02.130.
- [13] STAR Collaboration, "First Direct Measurement of Jets in $\sqrt{s_{NN}} = 200$ GeV Heavy Ion Collisions by STAR", *Eur. Phys. J.* **C61** (2009) 761, arXiv:0809.1609. doi:10.1140/epjc/s10052-009-0880-y.
- [14] STAR Collaboration, "First fragmentation function measurements from full jet reconstruction in heavy-ion collisions at $\sqrt{s_{NN}} = 200$ GeV by STAR", *Eur. Phys. J.* **C61** (2009) 629, arXiv:0809.1419. doi:10.1140/epjc/s10052-009-0904-7.
- [15] STAR Collaboration, "Measurements of jet structure and fragmentation from full jet reconstruction in heavy ion collisions at RHIC", *Nucl. Phys.* **A830** (2009) 267C, arXiv:0907.4788. doi:10.1016/j.nuclphysa.2009.10.097.
- [16] STAR Collaboration, "Inclusive cross section and correlations of fully reconstructed jets in 200 GeV Au+Au and p+p collisions", *Nucl. Phys.* **A830** (2009) 255C, arXiv:0908.1799. doi:10.1016/j.nuclphysa.2009.10.095.
- [17] D. A. Appel, "Jets as a probe of quark-gluon plasmas", *Phys. Rev.* **D33** (1986) 717. doi:10.1103/PhysRevD.33.717.
- [18] J. P. Blaizot and L. D. McLerran, "Jets in Expanding Quark - Gluon Plasmas", *Phys. Rev.* **D34** (1986) 2739. doi:10.1103/PhysRevD.34.2739.
- [19] ATLAS Collaboration, "Observation of a Centrality-Dependent Dijet Asymmetry in Lead-Lead Collisions at $\sqrt{s_{NN}} = 2.76$ TeV with the ATLAS Detector at the LHC", *Phys. Rev. Lett.* **105** (2010) 252303, arXiv:1011.6182.
- [20] CMS Collaboration, "The CMS experiment at the CERN LHC", *JINST* **3** (2008) S08004. doi:10.1088/1748-0221/3/08/S08004.
- [21] GEANT4 Collaboration, "GEANT4: A simulation toolkit", *Nucl. Instrum. Meth.* **A506** (2003) 250. doi:10.1016/S0168-9002(03)01368-8.
- [22] O. Djuvsland and J. Nystrand, "Single and Double Photonuclear Excitations in Pb+Pb Collisions at the LHC", arXiv:1011.4908.
- [23] CMS Collaboration, "Transverse-momentum and pseudorapidity distributions of charged hadrons in pp collisions at $\sqrt{s} = 7$ TeV", *Phys. Rev. Lett.* **105** (2010) 022002, arXiv:1005.3299. doi:10.1103/PhysRevLett.105.022002.
- [24] CMS Collaboration, "Electromagnetic calorimeter commissioning and performance with 7 TeV data", *CMS Note* **10-002** (2010).
- [25] CMS Collaboration, "Identification and Filtering of Uncharacteristic Noise in the CMS Hadron Calorimeter", *JINST* **5** (2010) T03014, arXiv:0911.4881. doi:10.1088/1748-0221/5/03/T03014.
- [26] M. L. Miller, K. Reygers, S. J. Sanders et al., "Glauber modeling in high energy nuclear collisions", *Ann. Rev. Nucl. Part. Sci.* **57** (2007) 205, arXiv:nucl-ex/0701025. doi:10.1146/annurev.nucl.57.090506.123020.

- [27] Z.-W. Lin, C. M. Ko, B.-A. Li et al., “A multi-phase transport model for relativistic heavy ion collisions”, *Phys. Rev.* **C72** (2005) 064901, arXiv:nucl-th/0411110. doi:10.1103/PhysRevC.72.064901.
- [28] H. De Vries, C. W. De Jager, and C. De Vries, “Nuclear charge and magnetization density distribution parameters from elastic electron scattering”, *Atom. Data Nucl. Data Tabl.* **36** (1987) 495.
- [29] Particle Data Group Collaboration, “Review of particle physics”, *J. Phys.* **G37** (2010) 075021. doi:10.1088/0954-3899/37/7A/075021.
- [30] O. Kodolova, I. Vardanian, A. Nikitenko et al., “The performance of the jet identification and reconstruction in heavy ions collisions with CMS detector”, *Eur. Phys. J.* **C50** (2007) 117. doi:10.1140/epjc/s10052-007-0223-9.
- [31] CMS Collaboration, “CMS technical design report, volume II: Physics performance”, *J. Phys.* **G34** (2007) 995. doi:10.1088/0954-3899/34/6/S01.
- [32] CMS Collaboration, “CMS physics: Technical Design Report Volume 1: Detector Performance and Software”, *CERN-LHCC-2006-001* (2006).
- [33] J. E. Huth, N. Wainer, K. Meier et al., “Toward a standardization of jet definitions”, in *Research Directions For The Decade: Snowmass '90*. 1990. FERMILAB-CONF-90-249-E.
- [34] CMS Collaboration, “Determination of the Jet Energy Scale in CMS with pp Collisions at $\sqrt{s} = 7$ TeV”, *CMS Physics Analysis Summary CMS-PAS-JME-10-010* (2010).
- [35] M. Cacciari, G. P. Salam, and G. Soyez, “The anti- k_t jet clustering algorithm”, *JHEP* **04** (2008) 063, arXiv:0802.1189. doi:10.1088/1126-6708/2008/04/063.
- [36] M. Cacciari, G. P. Salam, and G. Soyez, “The Catchment Area of Jets”, *JHEP* **0804** (2008) 005, arXiv:0802.1188. doi:10.1088/1126-6708/2008/04/005.
- [37] M. Cacciari and G. P. Salam, “Pileup subtraction using jet areas”, *Phys. Lett.* **B659** (2008) 119, arXiv:0707.1378. doi:10.1016/j.physletb.2007.09.077.
- [38] M. Cacciari, J. Rojo, G. P. Salam et al., “Jet Reconstruction in Heavy Ion Collisions”. 2010. arXiv:1010.1759.
- [39] CMS Collaboration, “Particle-Flow Event Reconstruction in CMS and Performance for Jets, Taus, and E_T^{miss} ”, *CMS Physics Analysis Summary CMS-PAS-PFT-09-001* (2009).
- [40] CMS Collaboration, “Commissioning of the Particle-Flow Reconstruction in Minimum-Bias and Jet Events from pp Collisions at 7 TeV”, *CMS Physics Analysis Summary CMS-PAS-PFT-10-002* (2010).
- [41] T. Sjöstrand, S. Mrenna, and P. Skands, “PYTHIA 6.4 Physics and Manual”, *JHEP* **05** (2006) 026 (tune D6T with PDFs CTEQ6L1 used for 2.76 TeV, tune Z2 for pp 7 TeV), arXiv:hep-ph/0603175.
- [42] I. P. Lokhtin and A. M. Snigirev, “A model of jet quenching in ultrarelativistic heavy ion collisions and high- p_T hadron spectra at RHIC”, *Eur. Phys. J.* **C45** (2006) 211, arXiv:hep-ph/0506189. doi:10.1140/epjc/s2005-02426-3.
- [43] M. Cacciari, G. P. Salam, and G. Soyez, “Fluctuations and asymmetric jet events in PbPb collisions at the LHC”, arXiv:1101.2878.

- [44] CMS Collaboration, “Jet Performance in pp Collisions at $\sqrt{s}=7$ TeV”, *CMS Physics Analysis Summary CMS-PAS-JME-10-003* (2010).
- [45] CMS Collaboration, CMS Collaboration, “Dijet Azimuthal Decorrelations in pp Collisions at $\sqrt{s} = 7$ TeV”. Submitted to *Physical Review Letters*, 2011. arXiv:1101.5029.

A The CMS Collaboration

Yerevan Physics Institute, Yerevan, Armenia

S. Chatrchyan, V. Khachatryan, A.M. Sirunyan, A. Tumasyan

Institut für Hochenergiephysik der OeAW, Wien, Austria

W. Adam, T. Bergauer, M. Dragicevic, J. Erö, C. Fabjan, M. Friedl, R. Frühwirth, V.M. Ghete, J. Hammer¹, S. Häseler, C. Hartl, M. Hoch, N. Hörmann, J. Hrubec, M. Jeitler, G. Kasieczka, W. Kiesenhofer, M. Krammer, D. Liko, I. Mikulec, M. Pernicka, H. Rohringer, R. Schöfbeck, J. Strauss, F. Teischinger, P. Wagner, W. Waltenberger, G. Walzel, E. Widl, C.-E. Wulz

National Centre for Particle and High Energy Physics, Minsk, Belarus

V. Mossolov, N. Shumeiko, J. Suarez Gonzalez

Universiteit Antwerpen, Antwerpen, Belgium

L. Benucci, E.A. De Wolf, X. Janssen, T. Maes, L. Mucibello, S. Ochesanu, B. Roland, R. Rougny, M. Selvaggi, H. Van Haevermaet, P. Van Mechelen, N. Van Remortel

Vrije Universiteit Brussel, Brussel, Belgium

S. Beauceron, F. Blekman, S. Blyweert, J. D'Hondt, O. Devroede, R. Gonzalez Suarez, A. Kalogeropoulos, J. Maes, M. Maes, W. Van Doninck, P. Van Mulders, G.P. Van Onsem, I. Villella

Université Libre de Bruxelles, Bruxelles, Belgium

O. Charaf, B. Clerbaux, G. De Lentdecker, V. Dero, A.P.R. Gay, G.H. Hammad, T. Hreus, P.E. Marage, L. Thomas, C. Vander Velde, P. Vanlaer, J. Wickens

Ghent University, Ghent, Belgium

V. Adler, S. Costantini, M. Grunewald, B. Klein, A. Marinov, J. Mccartin, D. Ryckbosch, F. Thyssen, M. Tytgat, L. Vanelderen, P. Verwilligen, S. Walsh, N. Zaganidis

Université Catholique de Louvain, Louvain-la-Neuve, Belgium

S. Basegmez, G. Bruno, J. Caudron, L. Ceard, E. Cortina Gil, C. Delaere, D. Favart, A. Giammanco, G. Grégoire, J. Hollar, V. Lemaître, J. Liao, O. Militaru, S. Ovyn, D. Pagano, A. Pin, K. Piotrkowski, N. Schul

Université de Mons, Mons, Belgium

N. Belyi, T. Caeberts, E. Daubie

Centro Brasileiro de Pesquisas Fisicas, Rio de Janeiro, Brazil

G.A. Alves, D. De Jesus Damiao, M.E. Pol, M.H.G. Souza

Universidade do Estado do Rio de Janeiro, Rio de Janeiro, Brazil

W. Carvalho, E.M. Da Costa, C. De Oliveira Martins, S. Fonseca De Souza, L. Mundim, H. Nogima, V. Oguri, W.L. Prado Da Silva, A. Santoro, S.M. Silva Do Amaral, A. Sznajder, F. Torres Da Silva De Araujo

Instituto de Fisica Teorica, Universidade Estadual Paulista, Sao Paulo, Brazil

F.A. Dias, T.R. Fernandez Perez Tomei, E. M. Gregores², F. Marinho, P.G. Mercadante², S.F. Novaes, Sandra S. Padula

Institute for Nuclear Research and Nuclear Energy, Sofia, Bulgaria

N. Darmanov¹, L. Dimitrov, V. Genchev¹, P. Iaydjiev¹, S. Piperov, M. Rodozov, S. Stoykova, G. Sultanov, V. Tcholakov, R. Trayanov, I. Vankov

University of Sofia, Sofia, Bulgaria

M. Dyulendarova, R. Hadjiiska, V. Kozhuharov, L. Litov, E. Marinova, M. Mateev, B. Pavlov, P. Petkov

Institute of High Energy Physics, Beijing, China

J.G. Bian, G.M. Chen, H.S. Chen, C.H. Jiang, D. Liang, S. Liang, X. Meng, J. Tao, J. Wang, J. Wang, X. Wang, Z. Wang, M. Xu, J. Zang, Z. Zhang

State Key Lab. of Nucl. Phys. and Tech., Peking University, Beijing, China

Y. Ban, S. Guo, Y. Guo, W. Li, Y. Mao, S.J. Qian, H. Teng, L. Zhang, B. Zhu, W. Zou

Universidad de Los Andes, Bogota, Colombia

A. Cabrera, B. Gomez Moreno, A.A. Ocampo Rios, A.F. Osorio Oliveros, J.C. Sanabria

Technical University of Split, Split, Croatia

N. Godinovic, D. Lelas, K. Lelas, R. Plestina³, D. Polic, I. Puljak

University of Split, Split, Croatia

Z. Antunovic, M. Dzelalija

Institute Rudjer Boskovic, Zagreb, Croatia

V. Brigljevic, S. Duric, K. Kadija, S. Morovic

University of Cyprus, Nicosia, Cyprus

A. Attikis, M. Galanti, J. Mousa, C. Nicolaou, F. Ptochos, P.A. Razis

Charles University, Prague, Czech Republic

M. Finger, M. Finger Jr.

Academy of Scientific Research and Technology of the Arab Republic of Egypt, Egyptian Network of High Energy Physics, Cairo, Egypt

Y. Assran⁴, S. Khalil⁵, M.A. Mahmoud⁶

National Institute of Chemical Physics and Biophysics, Tallinn, Estonia

A. Hektor, M. Kadastik, M. Müntel, M. Raidal, L. Rebane

Department of Physics, University of Helsinki, Helsinki, Finland

V. Azzolini, P. Eerola

Helsinki Institute of Physics, Helsinki, Finland

S. Czellar, J. Härkönen, V. Karimäki, R. Kinnunen, M.J. Kortelainen, T. Lampén, K. Lassila-Perini, S. Lehti, T. Lindén, P. Luukka, T. Mäenpää, E. Tuominen, J. Tuominiemi, E. Tuovinen, D. Ungaro, L. Wendland

Lappeenranta University of Technology, Lappeenranta, Finland

K. Banzuzi, A. Korpela, T. Tuuva

Laboratoire d'Annecy-le-Vieux de Physique des Particules, IN2P3-CNRS, Annecy-le-Vieux, France

D. Sillou

DSM/IRFU, CEA/Saclay, Gif-sur-Yvette, France

M. Besancon, S. Choudhury, M. Dejardin, D. Denegri, B. Fabbro, J.L. Faure, F. Ferri, S. Ganjour, F.X. Gentit, A. Givernaud, P. Gras, G. Hamel de Monchenault, P. Jarry, E. Locci, J. Malcles, M. Marionneau, L. Millischer, J. Rander, A. Rosowsky, I. Shreyber, M. Titov, P. Verrecchia

Laboratoire Leprince-Ringuet, Ecole Polytechnique, IN2P3-CNRS, Palaiseau, France

S. Baffioni, F. Beaudette, L. Benhabib, L. Bianchini, M. Bluj⁷, C. Broutin, P. Busson, C. Charlot, T. Dahms, L. Dobrzynski, S. Elgammal, R. Granier de Cassagnac, M. Haguenaer, P. Miné, C. Mironov, C. Ochando, P. Paganini, T. Roxlo, D. Sabes, R. Salerno, Y. Sirois, C. Thiebaut, B. Wyslouch⁸, A. Zabi

Institut Pluridisciplinaire Hubert Curien, Université de Strasbourg, Université de Haute Alsace Mulhouse, CNRS/IN2P3, Strasbourg, France

J.-L. Agram⁹, J. Andrea, D. Bloch, D. Bodin, J.-M. Brom, M. Cardaci, E.C. Chabert, C. Collard, E. Conte⁹, F. Drouhin⁹, C. Ferro, J.-C. Fontaine⁹, D. Gelé, U. Goerlach, S. Greder, P. Juillot, M. Karim⁹, A.-C. Le Bihan, Y. Mikami, P. Van Hove

Centre de Calcul de l'Institut National de Physique Nucleaire et de Physique des Particules (IN2P3), Villeurbanne, France

F. Fassi, D. Mercier

Université de Lyon, Université Claude Bernard Lyon 1, CNRS-IN2P3, Institut de Physique Nucléaire de Lyon, Villeurbanne, France

C. Baty, N. Beaupere, M. Bedjidian, O. Bondu, G. Boudoul, D. Boumediene, H. Brun, N. Chanon, R. Chierici, D. Contardo, P. Depasse, H. El Mamouni, A. Falkiewicz, J. Fay, S. Gascon, B. Ille, T. Kurca, T. Le Grand, M. Lethuillier, L. Mirabito, S. Perries, V. Sordini, S. Tosi, Y. Tschudi, P. Verdier, H. Xiao

E. Andronikashvili Institute of Physics, Academy of Science, Tbilisi, Georgia

L. Megrelidze

Institute of High Energy Physics and Informatization, Tbilisi State University, Tbilisi, Georgia

D. Lomidze

RWTH Aachen University, I. Physikalisches Institut, Aachen, Germany

G. Anagnostou, M. Edelhoff, L. Feld, N. Heracleous, O. Hindrichs, R. Jussen, K. Klein, J. Merz, N. Mohr, A. Ostapchuk, A. Perieanu, F. Raupach, J. Sammet, S. Schael, D. Sprenger, H. Weber, M. Weber, B. Wittmer

RWTH Aachen University, III. Physikalisches Institut A, Aachen, Germany

M. Ata, W. Bender, M. Erdmann, J. Frangenheim, T. Hebbeker, A. Hinzmann, K. Hoepfner, C. Hof, T. Klimkovich, D. Klingebiel, P. Kreuzer, D. Lanske[†], C. Magass, G. Masetti, M. Merschmeyer, A. Meyer, P. Papacz, H. Pieta, H. Reithler, S.A. Schmitz, L. Sonnenschein, J. Steggemann, D. Teyssier, M. Tonutti

RWTH Aachen University, III. Physikalisches Institut B, Aachen, Germany

M. Bontenackels, M. Davids, M. Duda, G. Flügge, H. Geenen, M. Giffels, W. Haj Ahmad, D. Heydhausen, T. Kress, Y. Kuessel, A. Linn, A. Nowack, L. Perchalla, O. Pooth, J. Rennefeld, P. Sauerland, A. Stahl, M. Thomas, D. Tornier, M.H. Zoeller

Deutsches Elektronen-Synchrotron, Hamburg, Germany

M. Aldaya Martin, W. Behrenhoff, U. Behrens, M. Bergholz¹⁰, K. Borrás, A. Cakir, A. Campbell, E. Castro, D. Dammann, G. Eckerlin, D. Eckstein, A. Flossdorf, G. Flucke, A. Geiser, J. Hauk, H. Jung, M. Kasemann, I. Katkov, P. Katsas, C. Kleinwort, H. Kluge, A. Knutsson, M. Krämer, D. Krücker, E. Kuznetsova, W. Lange, W. Lohmann¹⁰, R. Mankel, M. Marienfeld, I.-A. Melzer-Pellmann, A.B. Meyer, J. Mnich, A. Mussgiller, J. Olzem, D. Pitzl, A. Raspereza, A. Raval, M. Rosin, R. Schmidt¹⁰, T. Schoerner-Sadenius, N. Sen, A. Spiridonov, M. Stein, J. Tomaszewska, R. Walsh, C. Wissing

University of Hamburg, Hamburg, Germany

C. Autermann, S. Bobrovskiy, J. Draeger, H. Enderle, U. Gebbert, K. Kaschube, G. Kaussen, J. Lange, B. Mura, S. Naumann-Emme, F. Nowak, N. Pietsch, C. Sander, H. Schettler, P. Schleper, M. Schröder, T. Schum, J. Schwandt, H. Stadie, G. Steinbrück, J. Thomsen

Institut für Experimentelle Kernphysik, Karlsruhe, Germany

C. Barth, J. Bauer, V. Buege, T. Chwalek, W. De Boer, A. Dierlamm, G. Dirkes, M. Feindt, J. Gruschke, C. Hackstein, F. Hartmann, S.M. Heindl, M. Heinrich, H. Held, K.H. Hoffmann, S. Honc, T. Kuhr, D. Martschei, S. Mueller, Th. Müller, M. Niegel, O. Oberst, A. Oehler, J. Ott, T. Peiffer, D. Piparo, G. Quast, K. Rabbertz, F. Ratnikov, N. Ratnikova, M. Renz, C. Saout, A. Scheurer, P. Schieferdecker, F.-P. Schilling, M. Schmanau, G. Schott, H.J. Simonis, F.M. Stober, D. Troendle, J. Wagner-Kuhr, T. Weiler, M. Zeise, V. Zhukov¹¹, E.B. Ziebarth

Institute of Nuclear Physics "Demokritos", Aghia Paraskevi, Greece

G. Daskalakis, T. Geralis, K. Karafasoulis, S. Kesisoglou, A. Kyriakis, D. Loukas, I. Manolakos, A. Markou, C. Markou, C. Mavrommatis, E. Ntomari, E. Petrakou

University of Athens, Athens, Greece

L. Gouskos, T.J. Mertzimekis, A. Panagiotou

University of Ioánnina, Ioánnina, Greece

I. Evangelou, C. Foudas, P. Kokkas, N. Manthos, I. Papadopoulos, V. Patras, F.A. Triantis

KFKI Research Institute for Particle and Nuclear Physics, Budapest, Hungary

A. Aranyi, G. Bencze, L. Boldizsar, C. Hajdu¹, P. Hidas, D. Horvath¹², A. Kapusi, K. Krajczar¹³, F. Sikler, G.I. Veres¹³, G. Vesztergombi¹³

Institute of Nuclear Research ATOMKI, Debrecen, Hungary

N. Beni, J. Molnar, J. Palinkas, Z. Szillasi, V. Veszpremi

University of Debrecen, Debrecen, Hungary

P. Raics, Z.L. Trocsanyi, B. Ujvari

Panjab University, Chandigarh, India

S. Bansal, S.B. Beri, V. Bhatnagar, N. Dhingra, R. Gupta, M. Jindal, M. Kaur, J.M. Kohli, M.Z. Mehta, N. Nishu, L.K. Saini, A. Sharma, A.P. Singh, J.B. Singh, S.P. Singh

University of Delhi, Delhi, India

S. Ahuja, S. Bhattacharya, B.C. Choudhary, P. Gupta, S. Jain, S. Jain, A. Kumar, K. Ranjan, R.K. Shivpuri

Bhabha Atomic Research Centre, Mumbai, India

R.K. Choudhury, D. Dutta, S. Kailas, A.K. Mohanty¹, L.M. Pant, P. Shukla

Tata Institute of Fundamental Research - EHEP, Mumbai, India

T. Aziz, M. Guchait¹⁴, A. Gurtu, M. Maity¹⁵, D. Majumder, G. Majumder, K. Mazumdar, G.B. Mohanty, A. Saha, K. Sudhakar, N. Wickramage

Tata Institute of Fundamental Research - HECR, Mumbai, India

S. Banerjee, S. Dugad, N.K. Mondal

Institute for Research and Fundamental Sciences (IPM), Tehran, Iran

H. Arfaei, H. Bakhshiansohi, S.M. Etesami, A. Fahim, M. Hashemi, A. Jafari, M. Khakzad, A. Mohammadi, M. Mohammadi Najafabadi, S. Paktinat Mehdiabadi, B. Safarzadeh, M. Zeinali

INFN Sezione di Bari ^a, Università di Bari ^b, Politecnico di Bari ^c, Bari, Italy

M. Abbrescia^{a,b}, L. Barbone^{a,b}, C. Calabria^{a,b}, A. Colaleo^a, D. Creanza^{a,c}, N. De Filippis^{a,c}, M. De Palma^{a,b}, A. Dimitrov^a, L. Fiore^a, G. Iaselli^{a,c}, L. Lusito^{a,b,1}, G. Maggi^{a,c}, M. Maggi^a, N. Manna^{a,b}, B. Marangelli^{a,b}, S. My^{a,c}, S. Nuzzo^{a,b}, N. Pacifico^{a,b}, G.A. Pierro^a, A. Pompili^{a,b}, G. Pugliese^{a,c}, F. Romano^{a,c}, G. Roselli^{a,b}, G. Selvaggi^{a,b}, L. Silvestris^a, R. Trentadue^a, S. Tupputi^{a,b}, G. Zito^a

INFN Sezione di Bologna ^a, Università di Bologna ^b, Bologna, Italy

G. Abbiendi^a, A.C. Benvenuti^a, D. Bonacorsi^a, S. Braibant-Giacomelli^{a,b}, L. Brigliadori^a, P. Capiluppi^{a,b}, A. Castro^{a,b}, F.R. Cavallo^a, M. Cuffiani^{a,b}, G.M. Dallavalle^a, F. Fabbri^a, A. Fanfani^{a,b}, D. Fasanella^a, P. Giacomelli^a, M. Giunta^a, S. Marcellini^a, M. Meneghelli^{a,b}, A. Montanari^a, F.L. Navarria^{a,b}, F. Odoricci^a, A. Perrotta^a, F. Primavera^a, A.M. Rossi^{a,b}, T. Rovelli^{a,b}, G. Siroli^{a,b}, R. Travaglini^{a,b}

INFN Sezione di Catania ^a, Università di Catania ^b, Catania, Italy

S. Albergo^{a,b}, G. Cappello^{a,b}, M. Chiorboli^{a,b,1}, S. Costa^{a,b}, A. Tricomi^{a,b}, C. Tuve^a

INFN Sezione di Firenze ^a, Università di Firenze ^b, Firenze, Italy

G. Barbagli^a, V. Ciulli^{a,b}, C. Civinini^a, R. D'Alessandro^{a,b}, E. Focardi^{a,b}, S. Frosali^{a,b}, E. Gallo^a, S. Gonzi^{a,b}, P. Lenzi^{a,b}, M. Meschini^a, S. Paoletti^a, G. Sguazzoni^a, A. Tropiano^{a,1}

INFN Laboratori Nazionali di Frascati, Frascati, Italy

L. Benussi, S. Bianco, S. Colafranceschi¹⁶, F. Fabbri, D. Piccolo

INFN Sezione di Genova, Genova, Italy

P. Fabbriatore, R. Musenich

INFN Sezione di Milano-Bicocca ^a, Università di Milano-Bicocca ^b, Milano, Italy

A. Benaglia^{a,b}, F. De Guio^{a,b,1}, L. Di Matteo^{a,b}, A. Ghezzi^{a,b,1}, M. Malberti^{a,b}, S. Malvezzi^a, A. Martelli^{a,b}, A. Massironi^{a,b}, D. Menasce^a, L. Moroni^a, M. Paganoni^{a,b}, D. Pedrini^a, S. Ragazzi^{a,b}, N. Redaelli^a, S. Sala^a, T. Tabarelli de Fatis^{a,b}, V. Tancini^{a,b}

INFN Sezione di Napoli ^a, Università di Napoli "Federico II" ^b, Napoli, Italy

S. Buontempo^a, C.A. Carrillo Montoya^a, N. Cavallo^{a,17}, A. Cimmino^{a,b}, A. De Cosa^{a,b}, M. De Gruttola^{a,b}, F. Fabozzi^{a,17}, A.O.M. Iorio^a, L. Lista^a, M. Merola^{a,b}, P. Noli^{a,b}, P. Paolucci^a

INFN Sezione di Padova ^a, Università di Padova ^b, Università di Trento (Trento) ^c, Padova, Italy

P. Azzi^a, N. Bacchetta^a, P. Bellan^{a,b}, D. Bisello^{a,b}, A. Branca^a, R. Carlin^{a,b}, P. Checchia^a, M. De Mattia^{a,b}, T. Dorigo^a, U. Dosselli^a, F. Fanzago^a, F. Gasparini^{a,b}, U. Gasparini^{a,b}, S. Lacaprara^{a,18}, I. Lazzizzera^{a,c}, M. Margoni^{a,b}, M. Mazzucato^a, A.T. Meneguzzo^{a,b}, M. Nespolo^a, L. Perrozzi^{a,1}, N. Pozzobon^{a,b}, P. Ronchese^{a,b}, F. Simonetto^{a,b}, E. Torassa^a, M. Tosi^{a,b}, S. Vanini^{a,b}, P. Zotto^{a,b}, G. Zumerle^{a,b}

INFN Sezione di Pavia ^a, Università di Pavia ^b, Pavia, Italy

U. Berzano^a, S.P. Ratti^{a,b}, C. Riccardi^{a,b}, P. Vitulo^{a,b}

INFN Sezione di Perugia ^a, Università di Perugia ^b, Perugia, Italy

M. Biasini^{a,b}, G.M. Bilei^a, B. Caponeri^{a,b}, L. Fanò^{a,b}, P. Lariccia^{a,b}, A. Lucaroni^{a,b,1}, G. Mantovani^{a,b}, M. Menichelli^a, A. Nappi^{a,b}, A. Santocchia^{a,b}, S. Taroni^{a,b}, M. Valdata^{a,b}, R. Volpe^{a,b,1}

INFN Sezione di Pisa ^a, Università di Pisa ^b, Scuola Normale Superiore di Pisa ^c, Pisa, Italy

P. Azzurri^{a,c}, G. Bagliesi^a, J. Bernardini^{a,b}, T. Boccali^{a,1}, G. Broccolo^{a,c}, R. Castaldi^a, R.T. D'Agnolo^{a,c}, R. Dell'Orso^a, F. Fiori^{a,b}, L. Foà^{a,c}, A. Giassi^a, A. Kraan^a, F. Ligabue^{a,c},

T. Lomtadze^a, L. Martini^{a,19}, A. Messineo^{a,b}, F. Palla^a, F. Palmonari^a, G. Segneri^a, A.T. Serban^a, P. Spagnolo^a, R. Tenchini^a, G. Tonelli^{a,b,1}, A. Venturi^{a,1}, P.G. Verdini^a

INFN Sezione di Roma ^a, Università di Roma "La Sapienza" ^b, Roma, Italy

L. Barone^{a,b}, F. Cavallari^a, D. Del Re^{a,b}, E. Di Marco^{a,b}, M. Diemoz^a, D. Franci^{a,b}, M. Grassi^a, E. Longo^{a,b}, S. Nourbakhsh^a, G. Organtini^{a,b}, A. Palma^{a,b}, F. Pandolfi^{a,b,1}, R. Paramatti^a, S. Rahatlou^{a,b}

INFN Sezione di Torino ^a, Università di Torino ^b, Università del Piemonte Orientale (Novara) ^c, Torino, Italy

N. Amapane^{a,b}, R. Arcidiacono^{a,c}, S. Argiro^{a,b}, M. Arneodo^{a,c}, C. Biino^a, C. Botta^{a,b,1}, N. Cartiglia^a, R. Castello^{a,b}, M. Costa^{a,b}, N. Demaria^a, A. Graziano^{a,b,1}, C. Mariotti^a, M. Marone^{a,b}, S. Maselli^a, E. Migliore^{a,b}, G. Mila^{a,b}, V. Monaco^{a,b}, M. Musich^{a,b}, M.M. Obertino^{a,c}, N. Pastrone^a, M. Pelliccioni^{a,b,1}, A. Romero^{a,b}, M. Ruspa^{a,c}, R. Sacchi^{a,b}, V. Sola^{a,b}, A. Solano^{a,b}, A. Staiano^a, D. Trocino^{a,b}, A. Vilela Pereira^{a,b,1}

INFN Sezione di Trieste ^a, Università di Trieste ^b, Trieste, Italy

S. Belforte^a, F. Cossutti^a, G. Della Ricca^{a,b}, B. Gobbo^a, D. Montanino^{a,b}, A. Penzo^a

Kangwon National University, Chunchon, Korea

S.G. Heo, S.K. Nam

Kyungpook National University, Daegu, Korea

S. Chang, J. Chung, D.H. Kim, G.N. Kim, J.E. Kim, D.J. Kong, H. Park, S.R. Ro, D. Son, D.C. Son

Chonnam National University, Institute for Universe and Elementary Particles, Kwangju, Korea

Zero Kim, J.Y. Kim, S. Song

Korea University, Seoul, Korea

S. Choi, B. Hong, M. Jo, H. Kim, J.H. Kim, T.J. Kim, K.S. Lee, D.H. Moon, S.K. Park, H.B. Rhee, E. Seo, S. Shin, K.S. Sim

University of Seoul, Seoul, Korea

M. Choi, S. Kang, H. Kim, C. Park, I.C. Park, S. Park, G. Ryu

Sungkyunkwan University, Suwon, Korea

Y. Choi, Y.K. Choi, J. Goh, M.S. Kim, J. Lee, S. Lee, H. Seo, I. Yu

Vilnius University, Vilnius, Lithuania

M.J. Bilinskas, I. Grigelionis, M. Janulis, D. Martisiute, P. Petrov, T. Sabonis

Centro de Investigacion y de Estudios Avanzados del IPN, Mexico City, Mexico

H. Castilla-Valdez, E. De La Cruz-Burelo, R. Lopez-Fernandez, A. Sánchez-Hernández, L.M. Villasenor-Cendejas

Universidad Iberoamericana, Mexico City, Mexico

S. Carrillo Moreno, F. Vazquez Valencia

Benemerita Universidad Autonoma de Puebla, Puebla, Mexico

H.A. Salazar Ibarguen

Universidad Autónoma de San Luis Potosí, San Luis Potosí, Mexico

E. Casimiro Linares, A. Morelos Pineda, M.A. Reyes-Santos

University of Auckland, Auckland, New Zealand

D. Krofcheck

University of Canterbury, Christchurch, New Zealand

P.H. Butler, R. Doesburg, H. Silverwood

National Centre for Physics, Quaid-I-Azam University, Islamabad, Pakistan

M. Ahmad, I. Ahmed, M.I. Asghar, H.R. Hoorani, W.A. Khan, T. Khurshid, S. Qazi

Institute of Experimental Physics, Faculty of Physics, University of Warsaw, Warsaw, Poland

M. Cwiok, W. Dominik, K. Doroba, A. Kalinowski, M. Konecki, J. Krolikowski

Soltan Institute for Nuclear Studies, Warsaw, Poland

T. Frueboes, R. Gokieli, M. Górski, M. Kazana, K. Nawrocki, K. Romanowska-Rybinska, M. Szleper, G. Wrochna, P. Zalewski

Laboratório de Instrumentação e Física Experimental de Partículas, Lisboa, Portugal

N. Almeida, P. Bargassa, A. David, P. Faccioli, P.G. Ferreira Parracho, M. Gallinaro, P. Musella, A. Nayak, J. Seixas, J. Varela

Joint Institute for Nuclear Research, Dubna, Russia

S. Afanasiev, I. Belotelov, P. Bunin, I. Golutvin, A. Kamenev, V. Karjavin, G. Kozlov, A. Lanev, P. Moisenz, V. Palichik, V. Perehygin, S. Shmatov, V. Smirnov, A. Volodko, A. Zarubin

Petersburg Nuclear Physics Institute, Gatchina (St Petersburg), Russia

V. Golovtsov, Y. Ivanov, V. Kim, P. Levchenko, V. Murzin, V. Oreshkin, I. Smirnov, V. Sulimov, L. Uvarov, S. Vavilov, A. Vorobyev, A. Vorobyev

Institute for Nuclear Research, Moscow, Russia

Yu. Andreev, A. Dermenev, S. Gninenko, N. Golubev, M. Kirsanov, N. Krasnikov, V. Matveev, A. Pashenkov, A. Toropin, S. Troitsky

Institute for Theoretical and Experimental Physics, Moscow, Russia

V. Epshteyn, V. Gavrilov, V. Kaftanov[†], M. Kossov¹, A. Krokhotin, N. Lychkovskaya, V. Popov, G. Safronov, S. Semenov, V. Stolin, E. Vlasov, A. Zhokin

Moscow State University, Moscow, Russia

A. Ershov, A. Gribushin, O. Kodolova, V. Korotkikh, I. Lokhtin, S. Obraztsov, S. Petrushanko, A. Proskuryakov, L. Sarycheva, V. Savrin, A. Snigirev, I. Vardanyan

P.N. Lebedev Physical Institute, Moscow, Russia

V. Andreev, M. Azarkin, I. Dremin, M. Kirakosyan, A. Leonidov, S.V. Rusakov, A. Vinogradov

State Research Center of Russian Federation, Institute for High Energy Physics, Protvino, Russia

I. Azhgirey, S. Bitioukov, V. Grishin¹, V. Kachanov, D. Konstantinov, A. Korablev, V. Krychkine, V. Petrov, R. Ryutin, S. Slabospitsky, A. Sobol, L. Tourtchanovitch, S. Troshin, N. Tyurin, A. Uzunian, A. Volkov

University of Belgrade, Faculty of Physics and Vinca Institute of Nuclear Sciences, Belgrade, Serbia

P. Adzic²⁰, M. Djordjevic, D. Krpic²⁰, J. Milosevic

Centro de Investigaciones Energéticas Medioambientales y Tecnológicas (CIEMAT), Madrid, Spain

M. Aguilar-Benitez, J. Alcaraz Maestre, P. Arce, C. Battilana, E. Calvo, M. Cepeda, M. Cerrada, N. Colino, B. De La Cruz, A. Delgado Peris, C. Diez Pardos, D. Domínguez Vázquez, C. Fernandez Bedoya, J.P. Fernández Ramos, A. Ferrando, J. Flix, M.C. Fouz, P. Garcia-Abia,

O. Gonzalez Lopez, S. Goy Lopez, J.M. Hernandez, M.I. Josa, G. Merino, J. Puerta Pelayo, I. Redondo, L. Romero, J. Santaolalla, C. Willmott

Universidad Autónoma de Madrid, Madrid, Spain

C. Albajar, G. Codispoti, J.F. de Trocóniz

Universidad de Oviedo, Oviedo, Spain

J. Cuevas, J. Fernandez Menendez, S. Folgueras, I. Gonzalez Caballero, L. Lloret Iglesias, J.M. Vizan Garcia

Instituto de Física de Cantabria (IFCA), CSIC-Universidad de Cantabria, Santander, Spain

J.A. Brochero Cifuentes, I.J. Cabrillo, A. Calderon, M. Chamizo Llatas, S.H. Chuang, J. Duarte Campderros, M. Felcini²¹, M. Fernandez, G. Gomez, J. Gonzalez Sanchez, C. Jorda, P. Lobelle Pardo, A. Lopez Virto, J. Marco, R. Marco, C. Martinez Rivero, F. Matorras, F.J. Munoz Sanchez, J. Piedra Gomez²², T. Rodrigo, A.Y. Rodríguez-Marrero, A. Ruiz-Jimeno, L. Scodellaro, M. Sobron Sanudo, I. Vila, R. Vilar Cortabitarte

CERN, European Organization for Nuclear Research, Geneva, Switzerland

D. Abbaneo, E. Auffray, G. Auzinger, P. Baillon, A.H. Ball, D. Barney, A.J. Bell²³, D. Benedetti, C. Bernet³, W. Bialas, P. Bloch, A. Bocci, S. Bolognesi, M. Bona, H. Breuker, G. Brona, K. Bunkowski, T. Camporesi, G. Cerminara, J.A. Coarasa Perez, B. Curé, D. D'Enterria, A. De Roeck, S. Di Guida, A. Elliott-Peisert, B. Frisch, W. Funk, A. Gaddi, S. Gennai, G. Georgiou, H. Gerwig, D. Gigi, K. Gill, D. Giordano, F. Glege, R. Gomez-Reino Garrido, M. Gouzevitch, P. Govoni, S. Gowdy, L. Guiducci, M. Hansen, J. Harvey, J. Hegeman, B. Hegner, H.F. Hoffmann, A. Honma, V. Innocente, P. Janot, K. Kaadze, E. Karavakis, P. Lecoq, C. Lourenço, A. Macpherson, T. Mäki, L. Malgeri, M. Mannelli, L. Masetti, F. Meijers, S. Mersi, E. Meschi, R. Moser, M.U. Mozer, M. Mulders, E. Nesvold¹, M. Nguyen, T. Orimoto, L. Orsini, E. Perez, A. Petrilli, A. Pfeiffer, M. Pierini, M. Pimiä, G. Polese, A. Racz, J. Rodrigues Antunes, G. Rolandi²⁴, T. Rommerskirchen, C. Rovelli²⁵, M. Rovere, H. Sakulin, C. Schäfer, C. Schwick, I. Segoni, A. Sharma, P. Siegrist, M. Simon, P. Sphicas²⁶, M. Spiropulu²⁷, F. Stöckli, M. Stoye, P. Tropea, A. Tsiros, P. Vichoudis, M. Voutilainen, W.D. Zeuner

Paul Scherrer Institut, Villigen, Switzerland

W. Bertl, K. Deiters, W. Erdmann, K. Gabathuler, R. Horisberger, Q. Ingram, H.C. Kaestli, S. König, D. Kotlinski, U. Langenegger, F. Meier, D. Renker, T. Rohe, J. Sibille²⁸, A. Starodumov²⁹

Institute for Particle Physics, ETH Zurich, Zurich, Switzerland

P. Bortignon, L. Caminada³⁰, Z. Chen, S. Cittolin, G. Dissertori, M. Dittmar, J. Eugster, K. Freudenreich, C. Grab, A. Hervé, W. Hintz, P. Lecomte, W. Lustermann, C. Marchica³⁰, P. Martinez Ruiz del Arbol, P. Meridiani, P. Milenovic³¹, F. Moortgat, P. Nef, F. Nessi-Tedaldi, L. Pape, F. Pauss, T. Punz, A. Rizzi, F.J. Ronga, M. Rossini, L. Sala, A.K. Sanchez, M.-C. Sawley, B. Stieger, L. Tauscher[†], A. Thea, K. Theofilatos, D. Treille, C. Urscheler, R. Wallny, M. Weber, L. Wehrli, J. Weng

Universität Zürich, Zurich, Switzerland

E. Aguiló, C. Amsler, V. Chiochia, S. De Visscher, C. Favaro, M. Ivova Rikova, B. Millan Mejias, C. Regenfus, P. Robmann, A. Schmidt, H. Snoek

National Central University, Chung-Li, Taiwan

Y.H. Chang, E.A. Chen, K.H. Chen, W.T. Chen, S. Dutta, C.M. Kuo, S.W. Li, W. Lin, M.H. Liu, Z.K. Liu, Y.J. Lu, D. Mekterovic, J.H. Wu, S.S. Yu

National Taiwan University (NTU), Taipei, Taiwan

P. Bartalini, P. Chang, Y.H. Chang, Y.W. Chang, Y. Chao, K.F. Chen, W.-S. Hou, Y. Hsiung, K.Y. Kao, Y.J. Lei, R.-S. Lu, J.G. Shiu, Y.M. Tzeng, M. Wang

Cukurova University, Adana, Turkey

A. Adiguzel, Z. Demir, C. Dozen, I. Dumanoglu, E. Eskut, S. Girgis, G. Gokbulut, Y. Guler, E. Gurpinar, I. Hos, E.E. Kangal, T. Karaman, A. Kayis Topaksu, A. Nart, G. Onengut, K. Ozdemir, S. Ozturk, A. Polatoz, K. Sogut³², D. Sunar Cerci³³, D. Uzun, L.N. Vergili, M. Vergili, C. Zorbilmez

Middle East Technical University, Physics Department, Ankara, Turkey

I.V. Akin, T. Aliev, S. Bilmis, M. Deniz, H. Gamsizkan, A.M. Guler, K. Ocalan, A. Ozpineci, M. Serin, R. Sever, U.E. Surat, E. Yildirim, M. Zeyrek

Bogazici University, Istanbul, Turkey

M. Deliomeroğlu, D. Demir³⁴, E. Gülmez, A. Halu, B. Isildak, M. Kaya³⁵, O. Kaya³⁵, S. Ozkorucuklu³⁶, N. Sonmez³⁷

National Scientific Center, Kharkov Institute of Physics and Technology, Kharkov, Ukraine

L. Levchuk

University of Bristol, Bristol, United Kingdom

P. Bell, F. Bostock, J.J. Brooke, T.L. Cheng, E. Clement, D. Cussans, R. Frazier, J. Goldstein, M. Grimes, M. Hansen, D. Hartley, G.P. Heath, H.F. Heath, B. Huckvale, J. Jackson, L. Kreczko, S. Metson, D.M. Newbold³⁸, K. Nirunpong, A. Poll, S. Senkin, V.J. Smith, S. Ward

Rutherford Appleton Laboratory, Didcot, United Kingdom

L. Basso, K.W. Bell, A. Belyaev, C. Brew, R.M. Brown, B. Camanzi, D.J.A. Cockerill, J.A. Coughlan, K. Harder, S. Harper, B.W. Kennedy, E. Olaiya, D. Petyt, B.C. Radburn-Smith, C.H. Shepherd-Themistocleous, I.R. Tomalin, W.J. Womersley, S.D. Worm

Imperial College, London, United Kingdom

R. Bainbridge, G. Ball, J. Ballin, R. Beuselinck, O. Buchmuller, D. Colling, N. Cripps, M. Cutajar, G. Davies, M. Della Negra, J. Fulcher, D. Futyan, A. Guneratne Bryer, G. Hall, Z. Hatherell, J. Hays, G. Iles, G. Karapostoli, B.C. MacEvoy, A.-M. Magnan, J. Marrouche, R. Nandi, J. Nash, A. Nikitenko²⁹, A. Papageorgiou, M. Pesaresi, K. Petridis, M. Pioppi³⁹, D.M. Raymond, N. Rompotis, A. Rose, M.J. Ryan, C. Seez, P. Sharp, A. Sparrow, A. Tapper, M. Vazquez Acosta, T. Virdee, S. Wakefield, T. Whyntie

Brunel University, Uxbridge, United Kingdom

M. Barrett, M. Chadwick, J.E. Cole, P.R. Hobson, A. Khan, P. Kyberd, D. Leslie, W. Martin, I.D. Reid, L. Teodorescu

Baylor University, Waco, USA

K. Hatakeyama

Boston University, Boston, USA

T. Bose, E. Carrera Jarrin, C. Fantasia, A. Heister, J. St. John, P. Lawson, D. Lazic, J. Rohlf, D. Sperka, L. Sulak

Brown University, Providence, USA

A. Avetisyan, S. Bhattacharya, J.P. Chou, D. Cutts, A. Ferapontov, U. Heintz, S. Jabeen, G. Kukartsev, G. Landsberg, M. Narain, D. Nguyen, M. Segala, T. Speer, K.V. Tsang

University of California, Davis, Davis, USA

R. Breedon, M. Calderon De La Barca Sanchez, S. Chauhan, M. Chertok, J. Conway, P.T. Cox, J. Dolen, R. Erbacher, E. Friis, W. Ko, A. Kopecky, R. Lander, H. Liu, S. Maruyama, T. Miceli, M. Nikolic, D. Pellett, J. Robles, S. Salur, T. Schwarz, M. Searle, J. Smith, M. Squires, M. Tripathi, R. Vasquez Sierra, C. Veelken

University of California, Los Angeles, Los Angeles, USA

V. Andreev, K. Arisaka, D. Cline, R. Cousins, A. Deisher, J. Duris, S. Erhan, C. Farrell, J. Hauser, M. Ignatenko, C. Jarvis, C. Plager, G. Rakness, P. Schlein[†], J. Tucker, V. Valuev

University of California, Riverside, Riverside, USA

J. Babb, A. Chandra, R. Clare, J. Ellison, J.W. Gary, F. Giordano, G. Hanson, G.Y. Jeng, S.C. Kao, F. Liu, H. Liu, O.R. Long, A. Luthra, H. Nguyen, B.C. Shen[†], R. Stringer, J. Sturdy, S. Sumowidagdo, R. Wilken, S. Wimpenny

University of California, San Diego, La Jolla, USA

W. Andrews, J.G. Branson, G.B. Cerati, E. Dusinger, D. Evans, F. Golf, A. Holzner, R. Kelley, M. Lebourgeois, J. Letts, B. Mangano, S. Padhi, C. Palmer, G. Petrucciani, H. Pi, M. Pieri, R. Ranieri, M. Sani, V. Sharma¹, S. Simon, Y. Tu, A. Vartak, S. Wasserbaech, F. Würthwein, A. Yagil

University of California, Santa Barbara, Santa Barbara, USA

D. Barge, R. Bellan, C. Campagnari, M. D'Alfonso, T. Danielson, K. Flowers, P. Geffert, J. Incandela, C. Justus, P. Kalavase, S.A. Koay, D. Kovalskyi, V. Krutelyov, S. Lowette, N. Mccoll, V. Pavlunin, F. Rebassoo, J. Ribnik, J. Richman, R. Rossin, D. Stuart, W. To, J.R. Vlimant

California Institute of Technology, Pasadena, USA

A. Apresyan, A. Bornheim, J. Bunn, Y. Chen, M. Gataullin, Y. Ma, A. Mott, H.B. Newman, C. Rogan, V. Timciuc, P. Traczyk, J. Veverka, R. Wilkinson, Y. Yang, R.Y. Zhu

Carnegie Mellon University, Pittsburgh, USA

B. Akgun, R. Carroll, T. Ferguson, Y. Iiyama, D.W. Jang, S.Y. Jun, Y.F. Liu, M. Paulini, J. Russ, H. Vogel, I. Vorobiev

University of Colorado at Boulder, Boulder, USA

J.P. Cumalat, M.E. Dinardo, B.R. Drell, C.J. Edelmaier, W.T. Ford, A. Gaz, B. Heyburn, E. Luiggi Lopez, U. Nauenberg, J.G. Smith, K. Stenson, K.A. Ulmer, S.R. Wagner, S.L. Zang

Cornell University, Ithaca, USA

L. Agostino, J. Alexander, D. Cassel, A. Chatterjee, S. Das, N. Eggert, L.K. Gibbons, B. Heltsley, W. Hopkins, A. Khukhunaishvili, B. Kreis, G. Nicolas Kaufman, J.R. Patterson, D. Puigh, A. Ryd, X. Shi, W. Sun, W.D. Teo, J. Thom, J. Thompson, J. Vaughan, Y. Weng, L. Winstrom, P. Wittich

Fairfield University, Fairfield, USA

A. Biselli, G. Cirino, D. Winn

Fermi National Accelerator Laboratory, Batavia, USA

S. Abdullin, M. Albrow, J. Anderson, G. Apollinari, M. Atac, J.A. Bakken, S. Banerjee, L.A.T. Bauerdick, A. Beretvas, J. Berryhill, P.C. Bhat, I. Bloch, F. Borchering, K. Burkett, J.N. Butler, V. Chetluru, H.W.K. Cheung, F. Chlebana, S. Cihangir, W. Cooper, D.P. Eartly, V.D. Elvira, S. Esen, I. Fisk, J. Freeman, Y. Gao, E. Gottschalk, D. Green, K. Gunthoti, O. Gutsche, J. Hanlon, R.M. Harris, J. Hirschauer, B. Hooberman, H. Jensen, M. Johnson, U. Joshi, R. Khatiwada, B. Klima, K. Kousouris, S. Kunori, S. Kwan, C. Leonidopoulos,

P. Limon, D. Lincoln, R. Lipton, J. Lykken, K. Maeshima, J.M. Marraffino, D. Mason, P. McBride, T. Miao, K. Mishra, S. Mrenna, Y. Musienko⁴⁰, C. Newman-Holmes, V. O'Dell, R. Pordes, O. Prokofyev, N. Saoulidou, E. Sexton-Kennedy, S. Sharma, W.J. Spalding, L. Spiegel, P. Tan, L. Taylor, S. Tkaczyk, L. Uplegger, E.W. Vaandering, R. Vidal, J. Whitmore, W. Wu, F. Yang, F. Yumiceva, J.C. Yun

University of Florida, Gainesville, USA

D. Acosta, P. Avery, D. Bourilkov, M. Chen, G.P. Di Giovanni, D. Dobur, A. Drozdetskiy, R.D. Field, M. Fisher, Y. Fu, I.K. Furic, J. Gartner, S. Goldberg, B. Kim, J. Konigsberg, A. Korytov, A. Kropivnitskaya, T. Kypreos, K. Matchev, G. Mitselmakher, L. Muniz, Y. Pakhotin, C. Prescott, R. Remington, M. Schmitt, B. Scurlock, P. Sellers, N. Skhirtladze, D. Wang, J. Yelton, M. Zakaria

Florida International University, Miami, USA

C. Ceron, V. Gaultney, L. Kramer, L.M. Lebolo, S. Linn, P. Markowitz, G. Martinez, J.L. Rodriguez

Florida State University, Tallahassee, USA

T. Adams, A. Askew, D. Bandurin, J. Bochenek, J. Chen, B. Diamond, S.V. Gleyzer, J. Haas, V. Hagopian, M. Jenkins, K.F. Johnson, H. Prosper, L. Quertenmont, S. Sekmen, V. Veeraraghavan

Florida Institute of Technology, Melbourne, USA

M.M. Baarmand, B. Dorney, S. Guragain, M. Hohlmann, H. Kalakhety, R. Ralich, I. Vodopiyanov

University of Illinois at Chicago (UIC), Chicago, USA

M.R. Adams, I.M. Anghel, L. Apanasevich, Y. Bai, V.E. Bazterra, R.R. Betts, J. Callner, R. Cavanaugh, C. Dragoiu, L. Gauthier, C.E. Gerber, D.J. Hofman, S. Khalatyan, G.J. Kunde⁴¹, F. Lacroix, M. Malek, C. O'Brien, C. Silvestre, A. Smoron, D. Strom, N. Varelas

The University of Iowa, Iowa City, USA

U. Akgun, E.A. Albayrak, B. Bilki, W. Clarida, F. Duru, C.K. Lae, E. McCliment, J.-P. Merlo, H. Mermerkaya, A. Mestvirishvili, A. Moeller, J. Nachtman, C.R. Newsom, E. Norbeck, J. Olson, Y. Onel, F. Ozok, S. Sen, J. Wetzell, T. Yetkin, K. Yi

Johns Hopkins University, Baltimore, USA

B.A. Barnett, B. Blumenfeld, A. Bonato, C. Eskew, D. Fehling, G. Giurgiu, A.V. Gritsan, G. Hu, P. Maksimovic, S. Rappoccio, M. Swartz, N.V. Tran, A. Whitbeck

The University of Kansas, Lawrence, USA

P. Baringer, A. Bean, G. Benelli, O. Grachov, M. Murray, D. Noonan, S. Sanders, J.S. Wood, V. Zhukova

Kansas State University, Manhattan, USA

A.F. Barfuss, T. Bolton, I. Chakaberia, A. Ivanov, M. Makouski, Y. Maravin, S. Shrestha, I. Svintradze, Z. Wan

Lawrence Livermore National Laboratory, Livermore, USA

J. Gronberg, D. Lange, D. Wright

University of Maryland, College Park, USA

A. Baden, M. Boutemour, S.C. Eno, D. Ferencek, J.A. Gomez, N.J. Hadley, R.G. Kellogg, M. Kirn, Y. Lu, A.C. Mignerey, K. Rossato, P. Rumerio, F. Santanastasio, A. Skuja, J. Temple, M.B. Tonjes, S.C. Tonwar, E. Twedt

Massachusetts Institute of Technology, Cambridge, USA

B. Alver, G. Bauer, J. Bendavid, W. Busza, E. Butz, I.A. Cali, M. Chan, V. Dutta, P. Everaerts, G. Gomez Ceballos, M. Goncharov, K.A. Hahn, P. Harris, Y. Kim, M. Klute, Y.-J. Lee, W. Li, C. Loizides, P.D. Luckey, T. Ma, S. Nahn, C. Paus, D. Ralph, C. Roland, G. Roland, M. Rudolph, G.S.F. Stephans, K. Sumorok, K. Sung, E.A. Wenger, S. Xie, M. Yang, Y. Yilmaz, A.S. Yoon, M. Zanetti

University of Minnesota, Minneapolis, USA

P. Cole, S.I. Cooper, P. Cushman, B. Dahmes, A. De Benedetti, P.R. Duderu, G. Franzoni, J. Haupt, K. Klapoetke, Y. Kubota, J. Mans, V. Rekovic, R. Rusack, M. Sasseville, A. Singovsky

University of Mississippi, University, USA

L.M. Cremaldi, R. Godang, R. Kroeger, L. Perera, R. Rahmat, D.A. Sanders, D. Summers

University of Nebraska-Lincoln, Lincoln, USA

K. Bloom, S. Bose, J. Butt, D.R. Claes, A. Dominguez, M. Eads, J. Keller, T. Kelly, I. Kravchenko, J. Lazo-Flores, H. Malbouisson, S. Malik, G.R. Snow

State University of New York at Buffalo, Buffalo, USA

U. Baur, A. Godshalk, I. Iashvili, S. Jain, A. Kharchilava, A. Kumar, S.P. Shipkowski, K. Smith

Northeastern University, Boston, USA

G. Alverson, E. Barberis, D. Baumgartel, O. Boeriu, M. Chasco, S. Reucroft, J. Swain, D. Wood, J. Zhang

Northwestern University, Evanston, USA

A. Anastassov, A. Kubik, N. Odell, R.A. Ofierzynski, B. Pollack, A. Pozdnyakov, M. Schmitt, S. Stoynev, M. Velasco, S. Won

University of Notre Dame, Notre Dame, USA

L. Antonelli, D. Berry, M. Hildreth, C. Jessop, D.J. Karmgard, J. Kolb, T. Kolberg, K. Lannon, W. Luo, S. Lynch, N. Marinelli, D.M. Morse, T. Pearson, R. Ruchti, J. Slaunwhite, N. Valls, M. Wayne, J. Ziegler

The Ohio State University, Columbus, USA

B. Bylsma, L.S. Durkin, J. Gu, C. Hill, P. Killewald, K. Kotov, M. Rodenburg, G. Williams

Princeton University, Princeton, USA

N. Adam, E. Berry, P. Elmer, D. Gerbaudo, V. Halyo, P. Hebda, A. Hunt, J. Jones, E. Laird, D. Lopes Pegna, D. Marlow, T. Medvedeva, M. Mooney, J. Olsen, P. Piroué, X. Quan, H. Saka, D. Stickland, C. Tully, J.S. Werner, A. Zuranski

University of Puerto Rico, Mayaguez, USA

J.G. Acosta, X.T. Huang, A. Lopez, H. Mendez, S. Oliveros, J.E. Ramirez Vargas, A. Zatserklyaniy

Purdue University, West Lafayette, USA

E. Alagoz, V.E. Barnes, G. Bolla, L. Borrello, D. Bortoletto, A. Everett, A.F. Garfinkel, L. Gutay, Z. Hu, M. Jones, O. Koybasi, M. Kress, A.T. Laasanen, N. Leonardo, C. Liu, V. Maroussov, P. Merkel, D.H. Miller, N. Neumeister, I. Shipsey, D. Silvers, A. Svyatkovskiy, H.D. Yoo, J. Zablocki, Y. Zheng

Purdue University Calumet, Hammond, USA

P. Jindal, N. Parashar

Rice University, Houston, USA

C. Boulahouache, V. Cuplov, K.M. Ecklund, F.J.M. Geurts, B.P. Padley, R. Redjimi, J. Roberts, J. Zabel

University of Rochester, Rochester, USA

B. Betchart, A. Bodek, Y.S. Chung, R. Covarelli, P. de Barbaro, R. Demina, Y. Eshaq, H. Flacher, A. Garcia-Bellido, P. Goldenzweig, Y. Gotra, J. Han, A. Harel, D.C. Miner, D. Orbaker, G. Petrillo, D. Vishnevskiy, M. Zielinski

The Rockefeller University, New York, USA

A. Bhatti, R. Ciesielski, L. Demortier, K. Goulianos, G. Lungu, C. Mesropian, M. Yan

Rutgers, the State University of New Jersey, Piscataway, USA

O. Atramentov, A. Barker, D. Duggan, Y. Gershtein, R. Gray, E. Halkiadakis, D. Hidas, D. Hits, A. Lath, S. Panwalkar, R. Patel, A. Richards, K. Rose, S. Schnetzer, S. Somalwar, R. Stone, S. Thomas

University of Tennessee, Knoxville, USA

G. Cerizza, M. Hollingsworth, S. Spanier, Z.C. Yang, A. York

Texas A&M University, College Station, USA

J. Asaadi, R. Eusebi, J. Gilmore, A. Gurrola, T. Kamon, V. Khotilovich, R. Montalvo, C.N. Nguyen, I. Osipenkov, J. Pivarski, A. Safonov, S. Sengupta, A. Tatarinov, D. Toback, M. Weinberger

Texas Tech University, Lubbock, USA

N. Akchurin, J. Damgov, C. Jeong, K. Kovitanggoon, S.W. Lee, Y. Roh, A. Sill, I. Volobouev, R. Wigmans, E. Yazgan

Vanderbilt University, Nashville, USA

E. Appelt, E. Brownson, D. Engh, C. Florez, W. Gabella, M. Issah, W. Johns, P. Kurt, C. Maguire, A. Melo, P. Sheldon, S. Tuo, J. Velkovska

University of Virginia, Charlottesville, USA

M.W. Arenton, M. Balazs, S. Boutle, M. Buehler, S. Conetti, B. Cox, B. Francis, R. Hirosky, A. Ledovskoy, C. Lin, C. Neu, R. Yohay

Wayne State University, Detroit, USA

S. Gollapinni, R. Harr, P.E. Karchin, P. Lamichhane, M. Mattson, C. Milstène, A. Sakharov

University of Wisconsin, Madison, USA

M. Anderson, M. Bachtis, J.N. Bellinger, D. Carlsmith, S. Dasu, J. Efron, K. Flood, L. Gray, K.S. Grogg, M. Grothe, R. Hall-Wilton¹, M. Herndon, P. Klabbers, J. Klukas, A. Lanaro, C. Lazaridis, J. Leonard, R. Loveless, A. Mohapatra, D. Reeder, I. Ross, A. Savin, W.H. Smith, J. Swanson, M. Weinberg

†: Deceased

1: Also at CERN, European Organization for Nuclear Research, Geneva, Switzerland

2: Also at Universidade Federal do ABC, Santo Andre, Brazil

3: Also at Laboratoire Leprince-Ringuet, Ecole Polytechnique, IN2P3-CNRS, Palaiseau, France

4: Also at Suez Canal University, Suez, Egypt

5: Also at British University, Cairo, Egypt

6: Also at Fayoum University, El-Fayoum, Egypt

7: Also at Soltan Institute for Nuclear Studies, Warsaw, Poland

8: Also at Massachusetts Institute of Technology, Cambridge, USA

- 9: Also at Université de Haute-Alsace, Mulhouse, France
- 10: Also at Brandenburg University of Technology, Cottbus, Germany
- 11: Also at Moscow State University, Moscow, Russia
- 12: Also at Institute of Nuclear Research ATOMKI, Debrecen, Hungary
- 13: Also at Eötvös Loránd University, Budapest, Hungary
- 14: Also at Tata Institute of Fundamental Research - HECR, Mumbai, India
- 15: Also at University of Visva-Bharati, Santiniketan, India
- 16: Also at Facoltà Ingegneria Università di Roma "La Sapienza", Roma, Italy
- 17: Also at Università della Basilicata, Potenza, Italy
- 18: Also at Laboratori Nazionali di Legnaro dell' INFN, Legnaro, Italy
- 19: Also at Università degli studi di Siena, Siena, Italy
- 20: Also at Faculty of Physics of University of Belgrade, Belgrade, Serbia
- 21: Also at University of California, Los Angeles, Los Angeles, USA
- 22: Also at University of Florida, Gainesville, USA
- 23: Also at Université de Genève, Geneva, Switzerland
- 24: Also at Scuola Normale e Sezione dell' INFN, Pisa, Italy
- 25: Also at INFN Sezione di Roma; Università di Roma "La Sapienza", Roma, Italy
- 26: Also at University of Athens, Athens, Greece
- 27: Also at California Institute of Technology, Pasadena, USA
- 28: Also at The University of Kansas, Lawrence, USA
- 29: Also at Institute for Theoretical and Experimental Physics, Moscow, Russia
- 30: Also at Paul Scherrer Institut, Villigen, Switzerland
- 31: Also at University of Belgrade, Faculty of Physics and Vinca Institute of Nuclear Sciences, Belgrade, Serbia
- 32: Also at Mersin University, Mersin, Turkey
- 33: Also at Adiyaman University, Adiyaman, Turkey
- 34: Also at Izmir Institute of Technology, Izmir, Turkey
- 35: Also at Kafkas University, Kars, Turkey
- 36: Also at Suleyman Demirel University, Isparta, Turkey
- 37: Also at Ege University, Izmir, Turkey
- 38: Also at Rutherford Appleton Laboratory, Didcot, United Kingdom
- 39: Also at INFN Sezione di Perugia; Università di Perugia, Perugia, Italy
- 40: Also at Institute for Nuclear Research, Moscow, Russia
- 41: Also at Los Alamos National Laboratory, Los Alamos, USA